Current Biology

CellPress

Article

Mechanical and biochemical feedback combine to generate complex contractile oscillations in cytokinesis

Michael E. Werner,[1] Dylan D. Ray,[1] Coleman Breen,[1] Michael F. Staddon,[2] Florian Jug,[3] Shiladitya Banerjee,[4] and Amy Shaub Maddox[1,5,6,*]

[1]Department of Biology, University of North Carolina at Chapel Hill, Chapel Hill, NC 27599, USA
[2]Center for Systems Biology Dresden, Max Planck Institute for the Physics of Complex Systems, and Max Planck Institute of Molecular Cell Biology and Genetics, Dresden, Germany
[3]Computational Biology Research Centre, Human Technopole, Milan, Italy
[4]Department of Physics, Carnegie Mellon University, Pittsburgh, PA 15213, USA
[5]X (formerly Twitter): @AmyShaubMaddox
[6]Lead contact
*Correspondence: asm@unc.edu
https://doi.org/10.1016/j.cub.2024.06.037

SUMMARY

The actomyosin cortex is an active material that generates force to drive shape changes via cytoskeletal remodeling. Cytokinesis is the essential cell division event during which a cortical actomyosin ring closes to separate two daughter cells. Our active gel theory predicted that actomyosin systems controlled by a biochemical oscillator and experiencing mechanical strain would exhibit complex spatiotemporal behavior. To test whether active materials *in vivo* exhibit spatiotemporally complex kinetics, we imaged the *C. elegans* embryo with unprecedented temporal resolution and discovered that sections of the cytokinetic cortex undergo periodic phases of acceleration and deceleration. Contractile oscillations exhibited a range of periodicities, including those much longer periods than the timescale of RhoA pulses, which was shorter in cytokinesis than in any other biological context. Modifying mechanical feedback *in vivo* or *in silico* revealed that the period of contractile oscillation is prolonged as a function of the intensity of mechanical feedback. Fast local ring ingression occurs where speed oscillations have long periods, likely due to increased local stresses and, therefore, mechanical feedback. Fast ingression also occurs where material turnover is high, *in vivo* and *in silico*. We propose that downstream of initiation by pulsed RhoA activity, mechanical feedback, including but not limited to material advection, extends the timescale of contractility beyond that of biochemical input and, therefore, makes it robust to fluctuations in activation. Circumferential propagation of contractility likely allows for sustained contractility despite cytoskeletal remodeling necessary to recover from compaction. Thus, like biochemical feedback, mechanical feedback affords active materials responsiveness and robustness.

INTRODUCTION

The actomyosin cytoskeleton is an active material that generates contractile forces via the rearrangements and depolymerization of its motor, crosslinker, and polymer components. In non-muscle cells, actomyosin contractility is often activated by the molecular switch RhoA, which, in its active, guanosine triphosphate (GTP)-bound form, recruits and stimulates several downstream effectors that polymerize, crosslink, activate, and remodel the actomyosin cytoskeleton.[1] Cytoskeletal remodeling likely involves alignment, bundling, polarity sorting, sliding, and depolymerization of F-actin, but the relative preponderance and molecular mechanisms of these different events are unknown. RhoA is activated in a spatiotemporally specific manner by guanine nucleotide exchange factors (GEFs). Furthermore, RhoA is autocatalytic.[2–5] The RhoA effector Rho-associated kinase (Rho-K) phosphorylates and therefore activates the regulatory light chain of non-muscle myosin II (NMMII). The RhoA effector formin nucleates and promotes elongation of actin filaments (F-actin). Additionally, active RhoA recruits the scaffold protein anillin that binds F-actin, NMMII, and septins.[6–11] Together, these and other elements of the actomyosin cytoskeleton generate forces that maintain or change cell shape.[1,12–17]

While the positive regulation introduced above activates actomyosin, contractility is limited by and responsive to changing cues, via time-delayed negative feedback. F-actin promotes accumulation of a RhoA GTPase-activating protein (RhoGAP) that inhibits RhoA.[2,18–21] Via the heterodimeric kinase complex GCK-1/CCM-3, anillin promotes RhoA inhibition by RhoGAP.[22] In addition, RhoA is inhibited downstream of Rho-K.[23] Modeling biochemical circuits that include time-delayed negative feedback loops demonstrated that they generate excitability, oscillations, and traveling waves of active RhoA, its cytoskeletal effectors, and contractility.[2,18,19,24–27] Such phenomena have been

Please cite this article in press as: Werner et al., Mechanical and biochemical feedback combine to generate complex contractile oscillations in cytokinesis, Current Biology (2024), https://doi.org/10.1016/j.cub.2024.06.037

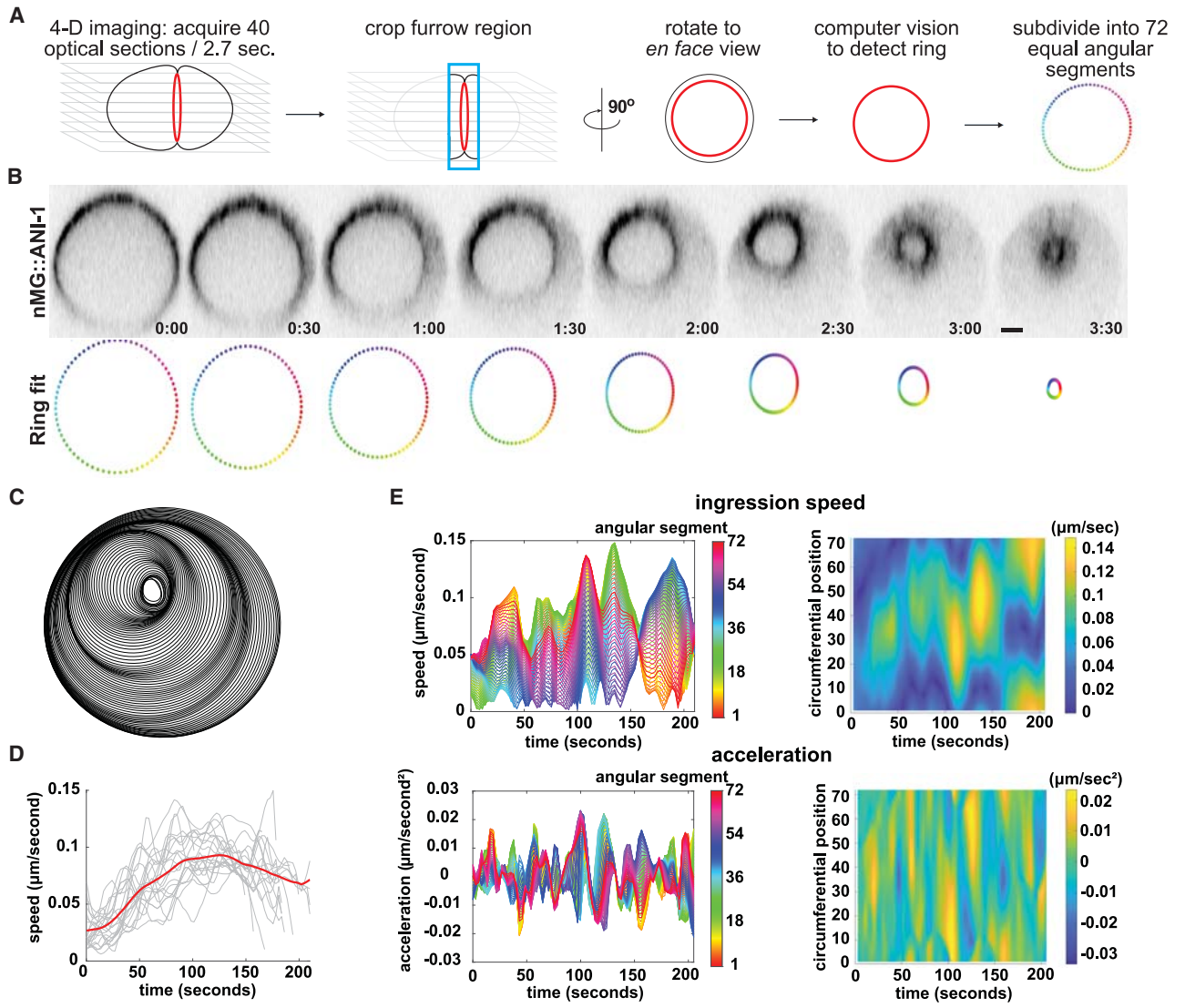

Figure 1. Cytokinetic rings exhibit local oscillation of ingression speed

(A) Computer vision pipeline to track cytokinetic ring ingression.

(B) *C. elegans* zygote cytokinetic ring labeled with mNG::ANI-1 (top) and fit polygons (bottom). Labels: minutes:seconds. Scale bar = 5 microns.

(C) All fit polygons for a representative cell.

(D) Mean cytokinetic ring ingression speed of all 5° angular segments. Mean speed for individual embryos (gray) and the population mean (red) (n = 22) (5 time point rolling average smoothing).

(E) Speed (top) and acceleration (bottom) of a representative cell. Left: speed for individual angular segments (color range). Right: colors represent speed or acceleration.

See also Figures S1 and S2 and Videos S1 and S2.

reported in diverse contexts including cell polarization, mitochondrial homeostasis, and cell division in fungi and animal cells.[24,25,28–32]

Superimposed on positive regulation and biochemical time-delayed negative feedback is mechanical feedback, in the form of advective flows that increase local concentrations of all cortical species.[33–37] Early theory work demonstrated that local accumulation of contractile cytoskeleton advects material centripetally, autocatalytically sustaining and amplifying small, transient local activation.[33] Furthermore, patterning of F-actin assembly via the lateral association of formin with F-actin,[38] cooperative binding of F-actin bundling proteins,[39–42] biased F-actin orientation according to the curvature of a membrane furrow,[43] and mechanoresponsive catch bonding and catch-slip bonding[44–50] all have the capacity to amplify the activation, accumulation, and rearrangements of the cytoskeleton, which comprise contractility.

Cytokinesis is an ancient and essential cell behavior in which localized activation of RhoA leads to the assembly and activation of the actomyosin cytoskeleton (Figure 1A). Cell-cycle progression

Please cite this article in press as: Werner et al., Mechanical and biochemical feedback combine to generate complex contractile oscillations in cytokinesis, Current Biology (2024), https://doi.org/10.1016/j.cub.2024.06.037

into anaphase and spatial patterning from the anaphase spindle lead to localized activation of RhoA via the conserved GEF ECT-2, in what is therefore the division plane.[51] As introduced above, active RhoA leads to contractility by recruiting, assembling, and activating the actomyosin cytoskeleton.[12] Once thought to be in a different, non-excitable regime during cytokinesis,[2,18] RhoA has recently been demonstrated to undergo time-delayed negative feedback in the division plane.[13,21] In addition, autocatalytic cortical flows during cytokinesis were modeled to amplify the localized signals of division plane specification.[33] At short length scales, material is drawn into contractile foci in some cell types.[52–54] Across the whole cell, material flows into the division plane as the cytokinetic ring assembles, contracts, and compacts.[34,35] Concomitant with concentration via flows, material is lost from the ring over the course of its closure.[35,55–59] The coexistence of biochemical feedback and mechanical feedback makes their combined effects difficult to predict.

Our model of the actomyosin cytoskeleton as an active gel revealed that the integration of mechanical feedback (e.g., due to advective cortical flows) with the well-characterized biochemical feedback loop is sufficient to generate complex patterns of contractility.[27] Such spatial and temporal asymmetries resemble complex contractile behaviors described in a variety of *in vivo* and reconstituted systems.[2,60–63] Because the cytokinetic ring operates under the control of the Rho-actomyosin time-delayed negative feedback loop and experiences cortical flows, we predicted that such complex spatiotemporal patterns occur in cytokinesis. However, the cytokinetic ring has been thought to simply operate at a maximum, and constant, speed.[57,59] We previously showed that rings in several animal cell types undergo acceleration and deceleration and exhibit spatial heterogeneities (unilateral closure) even without extrinsic mechanical constraints.[43,64–66] Higher temporal resolution was required to explore the existence of complex contractile patterns. Since the *C. elegans* zygote is mechanically and biochemically isolated within an eggshell and has a circular cross-section and centered anaphase spindle, it is an ideal model cell for the study of ring-intrinsic contractility.

We established methods to rapidly acquire image z series of entire *C. elegans* zygotes and the computer vision strategies required to annotate and analyze the resulting image datasets. Cytokinetic contractility exhibited repeated cycles of acceleration and deceleration. Prominent oscillations with short periods appeared to preserve the timescale of RhoA activation pulses, which have a unique timescale in this context. *In vivo* and *in silico*, the period of contractile oscillations was prolonged by the inclusion of mechanical feedback. Speed oscillations may represent cycles of compaction and remodeling that allow efficient and continual contractility. Our findings confirm predictions from theoretical work on the effects of combined biochemical and mechanical feedback on biological active materials.

RESULTS

The *C. elegans* cytokinetic ring undergoes contractile oscillations

The speed of cytokinetic ring contraction is routinely used as a proxy for ring performance. Speed has been variably reported to be constant or to gradually accelerate and decelerate.[57,59,64] By contrast, theory predicts that active gels like the actomyosin cytoskeleton, when subject to biochemical and mechanical feedback, undergo complex pulsatory dynamics and waves.[27] To explore whether such dynamics exist in the cytokinetic ring, we sought higher temporal resolution imaging of the entire ring. We imaged *C. elegans* zygotes expressing anillin fluorescently tagged at its endogenous locus (mNG::ANI-1[67]). To eliminate any artifacts resulting from cell compression,[68] embryos were mounted resting freely on the coverslip in a sealed chamber containing M9 buffer. An inverted resonant scanning confocal microscope was used to acquired 40 optical sections separated by 1 μm every 2.7 s. A semi-automated image analysis pipeline tracked ring closure dynamics over time (Figures 1A and 1B; Video S1).

Consistent with previous observations that ring closure is asymmetric in the zygote of *C. elegans* and other nematodes,[65,66,69] different regions of the ring ingressed at different speeds (Figures 1C and S1A). To capture circumferential variation in ring closure speed, we subdivided the ring into 72 equally spaced 5° angular segments and calculated closure speed with the distance between the position of any given segment at time point t and its position at time point t + 1, for each segment (Figures 1B and 1E). Individual ring segments did not ingress at constant speed, nor did they undergo a single gradual acceleration followed by deceleration, but they rather underwent repeated alternating phases of acceleration and deceleration (Figure 1E; Video S2). Speed oscillations were non-uniform around the ring circumference, varying in amplitude and speed, decelerating in some regions while accelerating elsewhere. The part of the cytokinetic ring that ingressed the fastest was not fixed in place, but instead it occupied a different position at different times during ring closure and traveled circumferentially (Figures 1C, 1E, and S1C; Video S2). We reason that speed oscillations have not been described previously because ring ingression speed has typically been calculated as change in diameter, which is often time-smoothed, and then averaged across multiple cells; these data treatments indeed obscure speed oscillations (Figure 1D).

A segment of the cytokinetic ring could undergo speed oscillations because the cytoskeleton in that region undergoes cycles of activation and inactivation under the local control of regulatory feedback loops. Alternatively, an assemblage of highly contractile cytoskeleton could travel circumferentially, causing local acceleration and deceleration as it entered and exited a given circumferential position. Some circumferential displacement of cortical material occurs during early anaphase in *C. elegans* zygotes that are compressed against the coverslip but is drastically reduced when compression is avoided.[68,70–72] To test whether the fastest-ingressing region of the ring travels circumferentially because the ring cytoskeleton physically moves around the ring circumference, we monitored the circumferential position of fiducial marks of mNG:ANI-1 in the cytokinetic ring. Local mNG::ANI-1 fluorescence inhomogeneities did not travel circumferentially but remained in approximately the same radial position throughout observation (Figures S1B–S1D). Since cytoskeletal material does not move circumferentially during ring closure in non-compressed cells, segments' speed oscillations and overall ring asymmetry likely occur because different regions of the ring are more contractile at different points in time. This

Please cite this article in press as: Werner et al., Mechanical and biochemical feedback combine to generate complex contractile oscillations in cytokinesis, Current Biology (2024), https://doi.org/10.1016/j.cub.2024.06.037

further supports the idea[57,73] that local assemblages of cytoskeleton respond semi-autonomously to local biochemical and mechanical signals.

Contractile speed oscillations was not an artifact of fluorescently tagging ANI-1 at its endogenous locus, as our observation held for cytokinetic rings visualized with endogenously fluorescently tagged non-muscle myosin (NMY-2::GFP) or Lifeact::mKate2 that labels F-actin (Figure S2A; data not shown). Contractile speed oscillations did not depend on asymmetric ring closure; they occurred in embryos depleted of either UNC-59 (septin) or ANI-1 (Figure S2B; data not shown), in which ring asymmetry is strongly reduced.[65] Speed oscillations were observed in various blastomeres in early *C. elegans* embryos and thus can occur across a range of initial cell sizes, fates, and degrees of adhesion, and they may be an inherent property of embryonic cytokinesis. In sum, the cytokinetic ring undergoes speed oscillations that qualitatively resemble the complex contractile fluctuations of a simulated active gel controlled by not only biochemical negative feedback but also mechanical feedback.

The cytokinetic ring contracts with a wide range of oscillation periods

Toward defining the regulation and mechanical underpinnings of contractile oscillations, and to compare this novel phenomenon in control and perturbed cells, we next sought to quantify the mechanical oscillations we observed. To do so, we measured the period and amplitude of the oscillations of individual segments. Qualitatively, oscillations appeared to be both amplitude and frequency modulated; so to capture variation in period and amplitude over time, we used wavelet synchrosqueezed transform (WSST) analysis that maximizes temporal resolution while also maximizing frequency space resolution[74,75] (Figure 2A). We first calculated acceleration to zero-center our data, and we fit the results of the WSST to an adaptive non-harmonic model (ANH).[74,76] This approach revealed the amplitude and period of several sinusoidal components (major modes) sufficient to reconstruct the input signal (>93% root-mean-square error [RMSE]; Figure 2B). We tabulated the incidence of all observed oscillation periods, weighting the counts by incidence and amplitude of each mode (see STAR Methods), to plot the distribution of oscillation frequencies present during ring ingression of control embryos (Figure 2C). Speed oscillations exhibited a wide range of periods. Since cytokinetic contractility is thought to be under the control of a single biochemical circuit, the coexistence of multiple oscillation periods suggested the existence of additional, coincident feedback loops.

Strain maintains and extends the oscillation period of a simulated active gel and in the cytokinetic ring

Modeled active gel representing the actomyosin cortex exhibits spatiotemporally irregular contractile oscillations.[27] The average period of this disordered contractility was 40 s when mechanical feedback, and therefore active contractile stress, was minimal, and it was longer (60 s) with higher stress.[27] Since contractile oscillations *in silico* qualitatively appeared disordered and heterogeneous, we sought to determine the range of oscillation periods that occur with mechanical feedback. To explore how strain and other variables affected the behavior of simulated actomyosin, we used our aforementioned published active gel model representing the actomyosin cortex, which was calibrated by *in vivo* measurements from *C. elegans* zygotes (Figure 3A).[27] Briefly, this model represents the contractile ring as a one-dimensional domain with periodic boundary conditions, comprising the reaction-diffusion dynamics of an excitable signaling network of RhoA and actomyosin, coupled to the mechanics of the actomyosin cytoskeleton (see STAR Methods). In this model, RhoA is activated by an input stimulus representing the RhoGEF ECT-2 and by autocatalytic positive feedback. An excitable RhoA signaling network generates "actomyosin," which represents F-actin, active NMMII, and the various cytoskeletal scaffold proteins (including anillin) that are recruited to the cortex downstream of RhoA. Actomyosin locally inhibits RhoA activity via time-delayed negative feedback. Simulating the cortex as a porous Maxwell viscoelastic material allows for the calculation of strain generation by actomyosin. Local actomyosin accumulation thus generates contractile stresses that lead to mechanical feedback, increasing the local concentrations of both actomyosin and RhoA via advective flow, which opposes the reaction and diffusion of RhoA and actomyosin (Figure 3A). We assumed that active contractile stress increases monotonically with actomyosin concentration, while saturating at higher actomyosin concentrations, consistent with *in vitro* observations in actomyosin networks.[77]

We first simulated the active gel with a spatially homogeneous stimulus of RhoGEF ECT-2 applied throughout the domain (Figure 3B) (see STAR Methods). With a sufficiently high stimulus, contractile material accumulated across the one-dimensional space, and after oscillating in abundance several times, it reached and remained at a level associated with active contractile stress σ_a[27] (Figure S3A). We then studied the effect of actomyosin-induced contractile stress σ_a on the spatiotemporal patterns of actomyosin. The spatiotemporal distribution of actomyosin material became increasingly complex with increasing σ_a, exhibiting irregular pulsatory dynamics (Figure S3A). Characterizing the period of the pulsatile contractility, using a simple Fourier transform at various levels of active contractile stress, revealed that as active stress σ_a was increased, the period of oscillations was higher on average and had a broader distribution (Figures 3C and S3A).

We next explored whether tuning active stress *in vivo* led to the same effect of higher average, and more complex, oscillation periods. In the mathematical model, mechanical feedback driven by contractile stress takes the form of advective flow, which counteracts the diffusion of RhoA and actomyosin. Thus, mechanical feedback is sensitive to changes in actomyosin contractility. To test if contractile oscillations in cytokinetic rings are sensitive to changes in mechanical feedback *in vivo*, we modulated contractile stress experimentally by tuning NMMII activity. We first depleted Rho-kinase (LET-502) by RNAi to reduce NMMII activity[78]; this treatment slowed cytokinetic ring closure (data not shown).[65] Rho-kinase-depleted cells exhibited speed oscillations with, on average, shorter periods (Figure 3D). A similar effect was observed following partial depletion of NMMII (NMY-2^{MHC}) (data not shown). We then increased NMMII activity by depleting the NMMII-binding subunit of the NMMII-inactivating phosphatase MEL-11^{MYPT}[78]; this condition shortened the duration of furrowing (data not shown).[78] In cells

Please cite this article in press as: Werner et al., Mechanical and biochemical feedback combine to generate complex contractile oscillations in cytokinesis, Current Biology (2024), https://doi.org/10.1016/j.cub.2024.06.037

CellPress

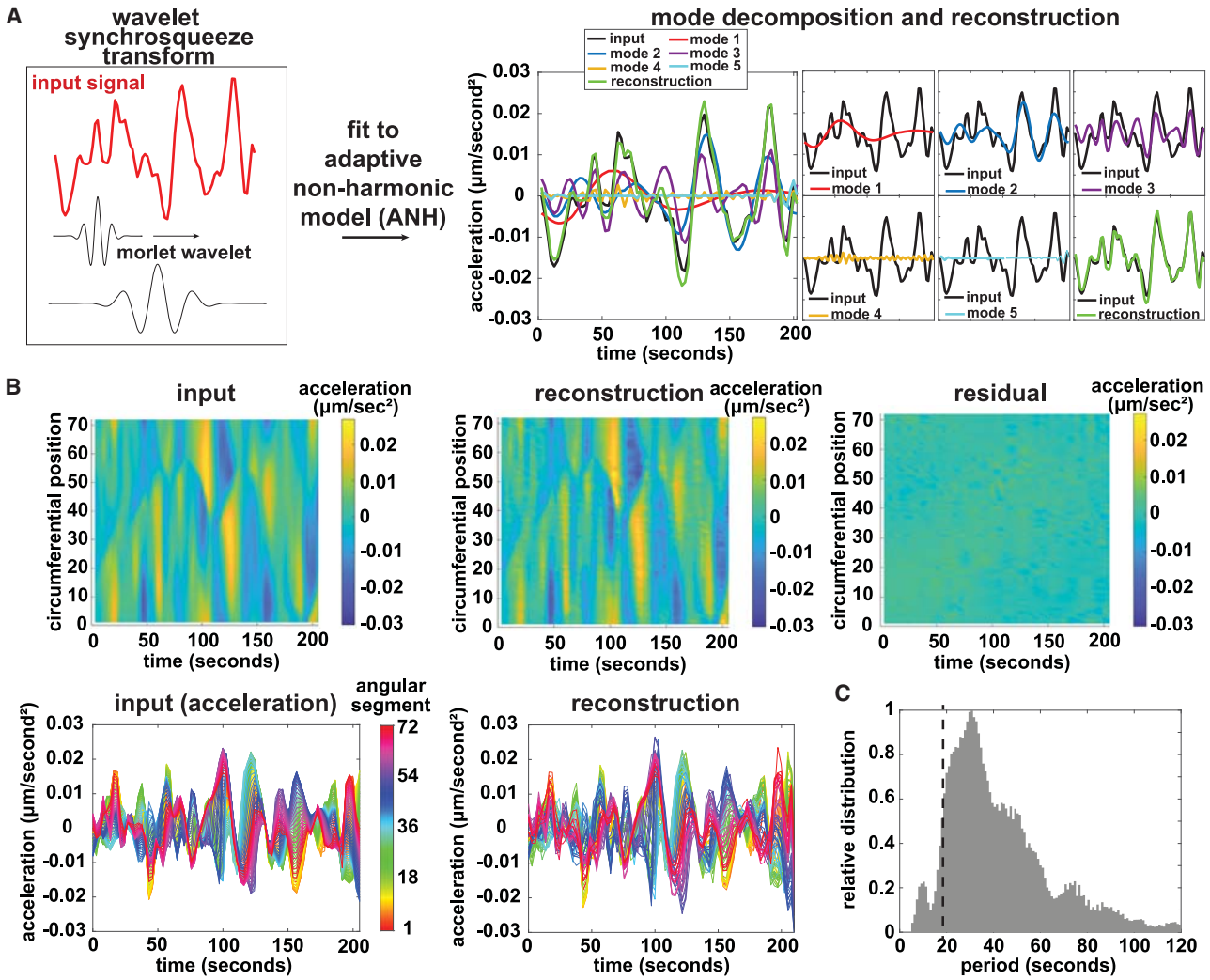

Figure 2. Wavelet analysis quantifies amplitude and period of contractile oscillations

(A) Left: input signal (red), Morlet wavelets (black). Right: modes (colors) that optimize reconstruction (green) of input signal are determined by fitting the data to an adaptive non-hormonic model (ANH).

(B) WSST and ANH of acceleration traces of 72 segments of a representative cell: input signal (left) reconstruction (middle) and residual (right).

(C) Control cell oscillation period distribution (n = 22 cells). Modes were adjusted by multiplying the amplitude by the inverse of its angular frequency. Dashed line: average period of LET-502 pulses.

See also Figures S4 and S6.

depleted of MEL-11, contractile oscillations had longer periods (Figure 3D). These results supported the conclusion that the long and varied periods of contractile oscillation in control cells reflect the strength of mechanical feedback.

Since depletion of conserved, essential proteins may confound observations, we sought a naturally occurring variation in contractility to test whether that variable was sufficient to explain differences in oscillation periods. In *C. elegans* blastomeres, tension increases over the course of cytokinetic ring closure.[79] We reasoned that this phenomenon also occurs in the zygote and compared speed oscillations between early and later furrowing in control embryos. During "involution," force is exerted in a broad band and mean furrowing speed is low, while during "furrowing" the initially rounded furrow adopts a sharp leading edge and mean ingression speed is higher.[80] Both the amplitude and period of oscillations were significantly higher during furrowing than during involution (Figure 3E). These findings align with the prediction made by modulating active stress *in silico*, and they support the idea that contractility is highly complex in cytokinesis due to mechanical feedback.

Contractile oscillations preserve and extend the timescale of RhoA activity pulses

The biochemical oscillator circuit wherein active RhoA elicits actomyosin activation and assembly, which in turn inhibits RhoA, has a characteristic timescale in each context where it has been examined. In pulses and waves, the abundance of active RhoA and its cytoskeletal effectors rise from and fall back to undetectable levels in 30–120 s, depending on the cell type.[2,19,21,22,26,37] In the *C. elegans* zygote undergoing

Please cite this article in press as: Werner et al., Mechanical and biochemical feedback combine to generate complex contractile oscillations in cytokinesis, Current Biology (2024), https://doi.org/10.1016/j.cub.2024.06.037

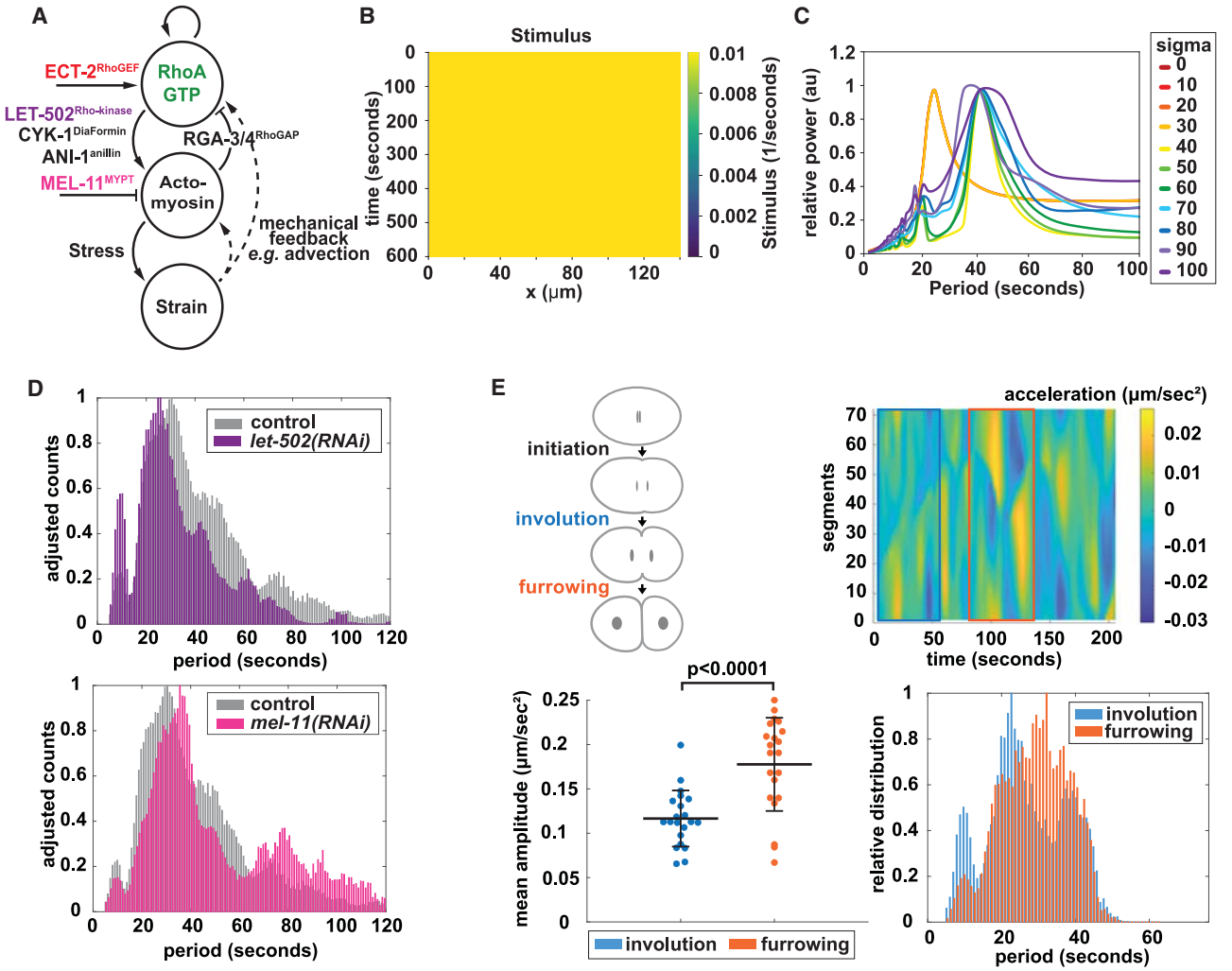

Figure 3. Mechanical feedback prolongs oscillation periods *in silico* and *in vivo*

(A) Schematic of simulated feedback loops highlighting point of action of NMMII regulators.

(B) Kymograph of simulated continuous stimulus.

(C) Frequency spectra of individual Fourier transforms, quantifying oscillation periods of simulated actomyosin contractile waves with different levels of strain (sigma).

(D) Adjusted period profiles of control and *let-502(RNAi)* embryos (n = 10) (top) and control and *mel-11(RNAi)* embryos (n = 10) (bottom).

(E) Stages of cytokinesis in *C. elegans* cytokinesis (top left). Amplitude (bottom left) and period profiles (bottom right) of speed oscillation during involution (blue; furrow initiation + 55 s) and furrowing (orange; 81–135 s after furrow initiation) (top right).

See also Figure S3.

polarization during mitotic prophase, the contractile pulse timescale is 30–35 s.[19,37]

To determine the timescale of the biochemical circuit driving cytoskeletal activation and assembly, and RhoA inhibition, in cytokinesis, we visualized active RhoA by using GFP::LET-502, a *bona fide* measure of Rho activity (Figures 4A and 4B).[22] Despite the circumferential cortical rotation around the embryo long axis in early anaphase that resulted from gentle compression,[68,71] active RhoA appeared in transient cortical patches in early anaphase, primarily in the cell equator. NMMII appeared in the same patches, following a delay (Figure 4B; Video S3). The timescale of RhoA cortical patch persistence ranged from approximately 15 to 22 s, with an average of approximately 18 s (Figure 4C). This timescale is shorter than that of pulses during polarization, suggesting that the reactions and interactions that drive this conserved biochemical circuit differ between cell-cycle phases in *C. elegans* embryos, as does the period of cortical actomyosin waves in other animal cell types.[19,21,26,37,81]

To test how contractile speed oscillations relate to the intensity of biochemical feedback, we decreased RhoA activity by depleting the RhoGEF ECT-2, which causes reduced cortical accumulation of LET-502[22,82] and slows cytokinetic ring closure.[3,83] The amplitude of contractile speed oscillations was decreased following ECT-2 depletion (Figure 4D). The distributions of the periods of contractile speed oscillations were also affected by lowering RhoA activity: shorter periods were

Please cite this article in press as: Werner et al., Mechanical and biochemical feedback combine to generate complex contractile oscillations in cytokinesis, Current Biology (2024), https://doi.org/10.1016/j.cub.2024.06.037

CellPress

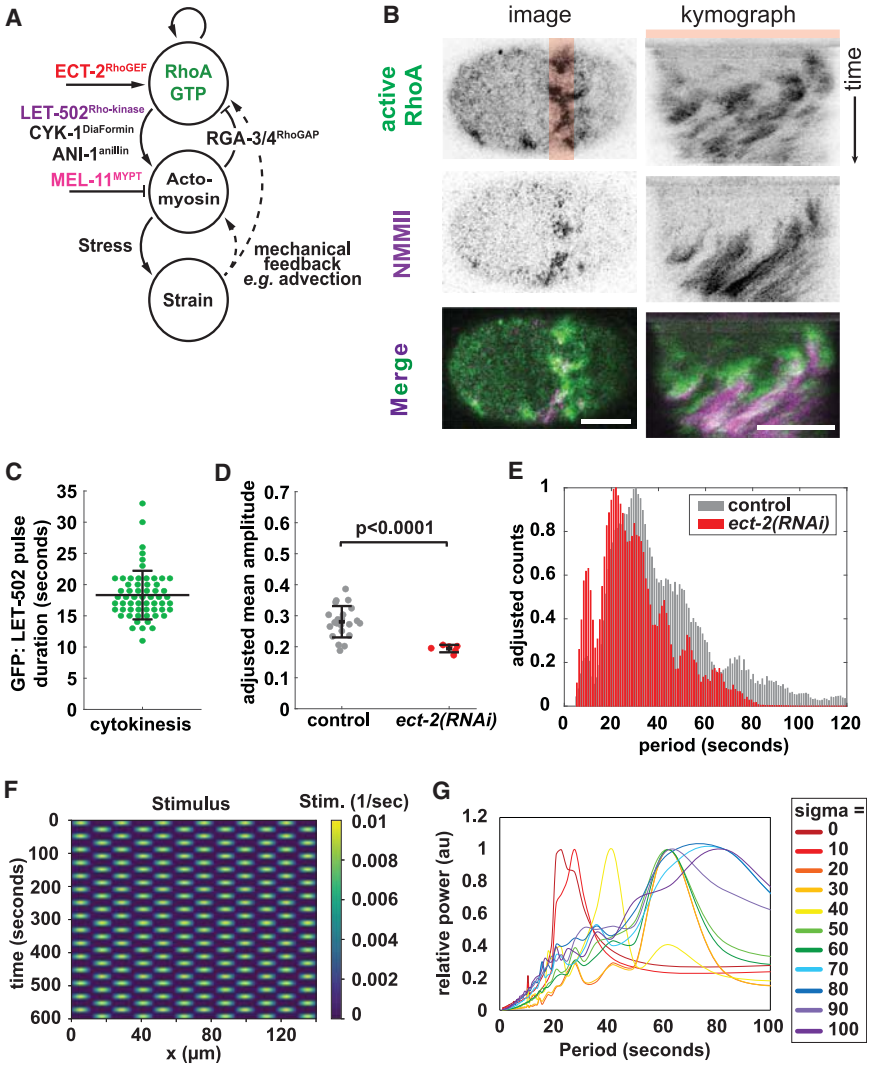

Figure 4. Local speed oscillations are sensitive to changes in the amount of RhoA activity, which pulses in the cell equator

(A) Schematic of simulated feedback loops. Colors depict protein depletion targets.

(B) *C. elegans* zygote at furrow onset expressing RhoA activity sensor GFP::LET-502 (top, green) and NMY-2::RFP (middle, magenta; bottom: merge). Kymograph of red highlighted area (right). Scale bars = 10 microns.

(C) Period of GFP-LET-502 pulses in the equator during anaphase (n = 51 foci from 10 embryos).

(D) Adjusted mean amplitude of speed oscillations in control (n = 21) and partially ECT-2-depleted cells with reduced ingression speed (n = 6). Data points: mean amplitude of a single embryo.

(E) Adjusted period profiles of control and partial *ect-2(RNAi)* cells with reduced ingression speed.

(F) Kymograph of the simulated pulsatile stimulus.

(G) Frequency spectra of Fourier transforms, quantifying oscillation periods of simulated actomyosin contractile waves with different levels of mechanical feedback (sigma).

See also Figure S6 and Video S3.

over-represented and longer periods occurred less, as compared with the distribution of periods in control cells (Figure 4E). The response of contractile oscillation period to modulating RhoA pulses suggests that the former is a function of the latter.

Given the importance of RhoA activation for driving contractility, we next considered how, *in vivo*, the RhoA-actomyosin circuit becomes activated in distinct foci, not uniformly as we initially modeled.[27] To add realism to our simulations, we modeled the effects of a locally focused, pulsed stimulus (Figure 4F; see STAR Methods). In the absence of mechanical feedback (σ_a = 0), the period of the input stimulus was preserved and slightly extended by the accumulation of contractile material. When mechanical feedback and therefore low active contractile stress σ_a was included, the period of the response doubled. Higher active stress caused even more disordered contractility, mimicking the propagating waves and contractile flows reported previously.[27] Longer periods were increasingly represented with increased stress (Figures 4G and S3B), as for active gel with homogeneous input stimulus (Figures 3C and S3A). These results demonstrate that mechanical feedback can prolong pulsatile contraction beyond the period of a pulsed stimulus. These simulations thus further suggest that *in vivo*, the short-period contractile oscillations we observe arise from the preservation of the timescale of the RhoA circuit and that, in a stress-dependent manner, longer-period oscillations emerge.

Efficiently contracting cytoskeleton exhibits robust actomyosin accumulation and slow oscillation

The mechanical feedback loops implemented in our mathematical model act by advecting (gathering) biochemical regulators and cytoskeletal elements.[27] This concept predicts that contractility is optimal, and hence produces the maximal contractile force, where the rate of increase of network components is the highest. We thus next tested whether this occurs *in vivo* by comparing the position of the fastest-ingressing segment with the region with the largest instantaneous increase in ANI-1 or NMY-2 accumulation. Indeed, the fastest-ingressing part of the ring exhibited significantly higher rates of both ANI-1 and NMY-2 accumulation (Figures 5A, 5B, and S4). These results suggest that cytokinetic ring remodeling via advective flows promotes contractility.

Since advection and the resulting material compaction appear to locally generate more stress,[62,84–88] we next tested whether regions of rapid material accumulation and high ingression speed experience longer speed oscillations. Comparing regions of the ring undergoing fastest ingression with those moving slowest revealed that the fast-ingressing segments oscillated with a significantly higher period than did slow-moving segments (Figure 5C). This correlation suggests that high amplitude, long-period speed oscillations promote contractility.

Please cite this article in press as: Werner et al., Mechanical and biochemical feedback combine to generate complex contractile oscillations in cytokinesis, Current Biology (2024), https://doi.org/10.1016/j.cub.2024.06.037

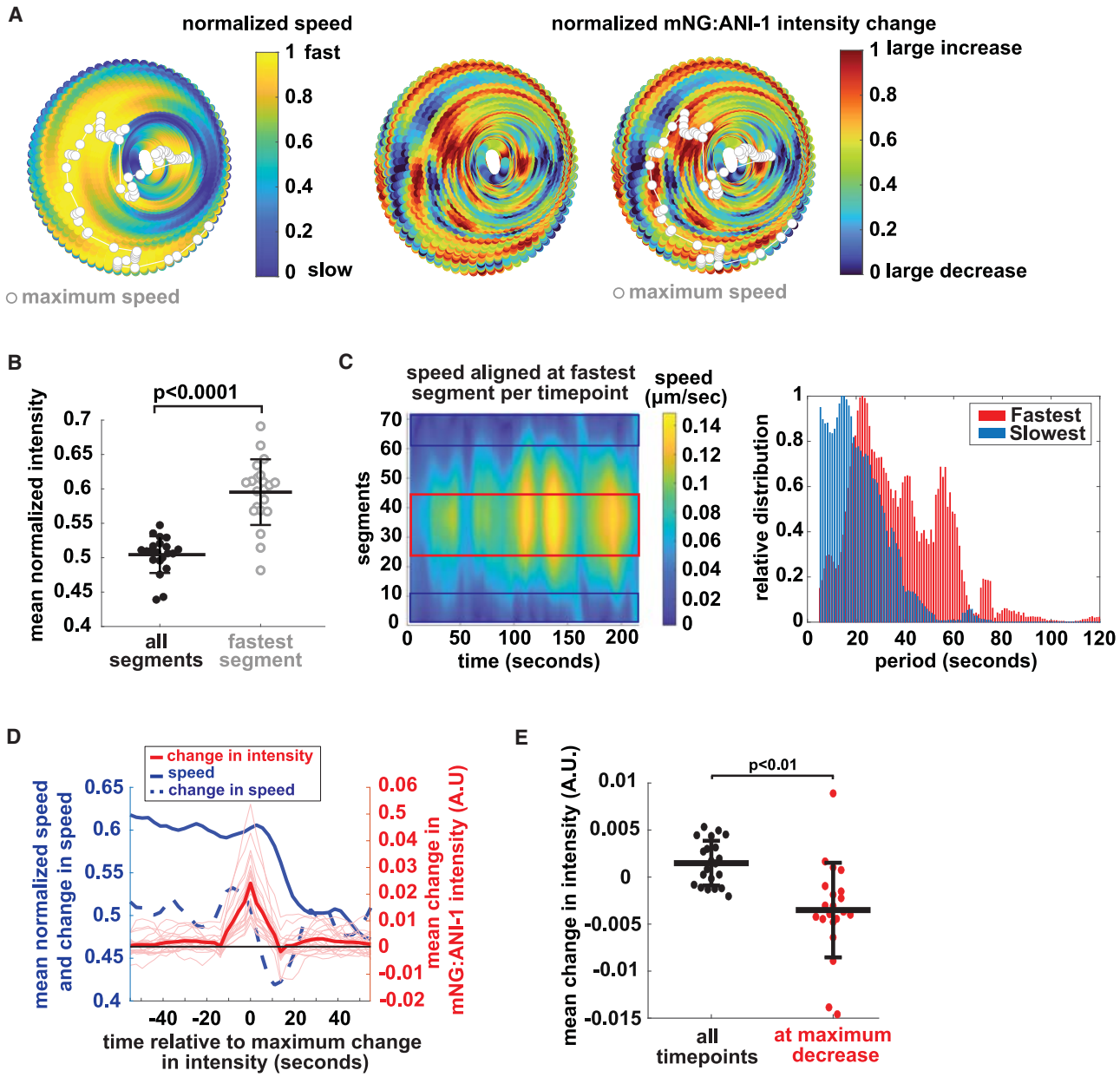

Figure 5. The fastest-ingressing region of the cytokinetic ring exhibits the largest local increases of ANI-1 density

(A) Circular kymographs showing local normalized ingression speed overlayed with the position of the fastest traveling segment at each time point (white/gray, left), local normalized change in mNG-ANI-1 fluorescence intensity (middle), and normalized change in fluorescence intensity overlayed with the position of the fastest traveling segment at each time point (white/gray; right). Each point represents a 5° angular segment.

(B) Mean normalized change in intensity for all segments and the fastest-ingressing angular segment only. Data points represent the mean value for all time points of an individual embryo (n = 21).

(C) Period distribution (right) of the 20 fastest (red) and the 20 slowest (blue) traveling segments after aligning segments at the fastest traveling segment at each time point (left).

(D) Mean change in mNeonGreen::ANI-1 intensity in time points preceding (negative x values) and following (positive x values) a local segment reaching maximum increase in mNeonGreen::ANI-1 levels (red: population mean, pink: means for individual embryos [right y axis]). Mean normalized speed (solid blue line, left y axis) and mean normalized acceleration (dotted blue line, left y axis) at the corresponding time points.

(E) Mean change in intensity for all time points (black) and ~16 s after reaching maximum change in intensity only (red).

See also Figures S4 and S5.

Please cite this article in press as: Werner et al., Mechanical and biochemical feedback combine to generate complex contractile oscillations in cytokinesis, Current Biology (2024), https://doi.org/10.1016/j.cub.2024.06.037

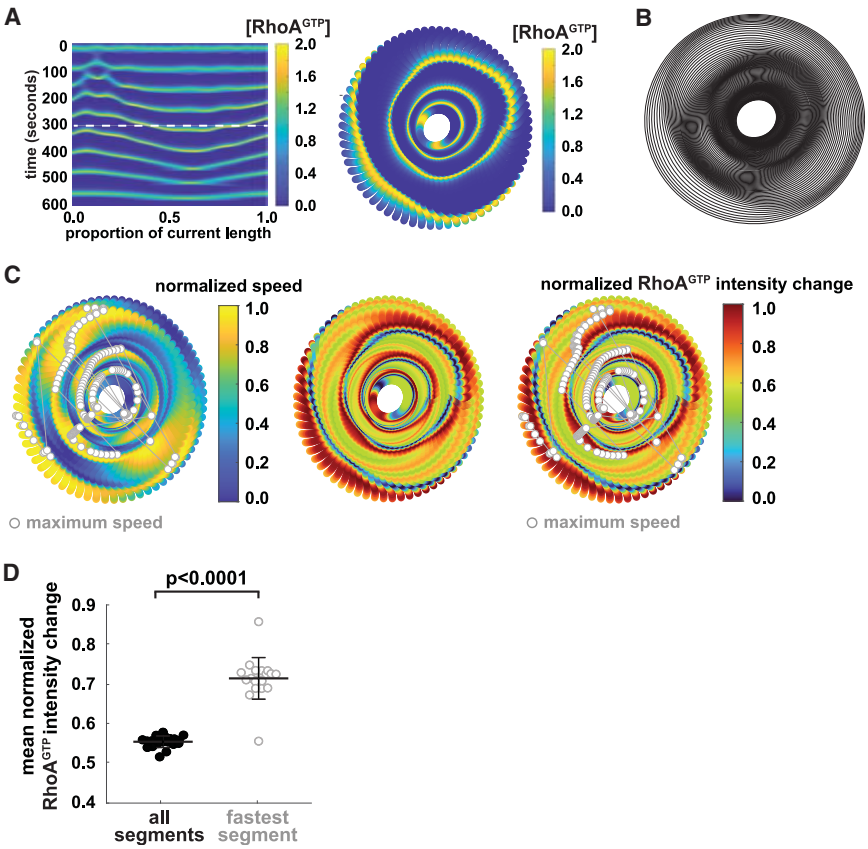

Figure 6. A simulated contractile ring of active gel exhibits physiologically realistic features

Simulated active gel was allowed to shrink concentrically starting 300 s after the start of the simulation (white dashed line in A). All diagrams except for (A) show simulation results of a representative simulation between 300 and 500 s following the start of the simulation. Simulation parameters: strain sigma = 40, stimulus Sr = 0.01, friction in the radial direction gamma_radial = 10, starting ring radius = 15 μm.

(A) Kymograph (left, entire simulation) and circular kymograph (right, 300–500 s) of active RhoA concentration.

(B) Evolution of simulated rings over time (every other time point shown).

(C) Circular kymographs of normalized ingression speed; gray: fastest-ingressing segment (left and right), normalized change in RhoA concentration (above 0.5 = increase; below 0.5 = decrease) (middle and right).

(D) Mean normalized change in active RhoA concentration for all segments (black) and the fastest-ingressing angular segment only (gray). Points: mean value for all time points between 300 and 500 s of an individual simulation (n = 20).

See also Video S4.

The continuous local increase of contractile material via mechanical feedback is expected to begin to oppose local contraction when the amount of non-motor crosslinker exceeds the threshold for optimal constriction.[62,84–87] Increased mechanical stress on the actomyosin network could cause filament buckling and loss of contractile material from the ring.[1,56,89–91] To assess the relationship between contractile material density and ingression velocity, we compared local material density change (mNeonGreen::ANI-1 or NMY-2::GFP) and segment ingression speed. Segments with the highest rate of decrease in ANI-1 or NMY-2 density moved more slowly than the average segment (Figure S5A). Similarly, slow segments underwent less material recruitment/compaction than the average segment (Figure S5B).

To describe the sequence of events in a contractile pulse, we identified the segment with the highest increase in material density for each time point and followed this segment over time. The rate of ANI-1 or NMY-2 accumulation sharply increased and then decreased, likely reflecting a preceding (by 10 s) pulse of RhoA activity as shown previously.[19] As the local material density increased, contractility first accelerated. Within one time point (2.7 s) of when the rate of ANI-1 or NMY-2 density change peaked, contractility began to decelerate. Approximately 16 s after peaking, the rate of accumulation of ANI-1 or NMY-2 turned negative for several time points (Figures 5D, 5E, S5C, and S5D), indicative of a temporary local net loss of cytoskeletal material.

Our analyses suggest that contractile speed oscillations represent repeating cycles of activation, compaction, and remodeling. Specifically, they predict that the fastest-ingressing part of the ring cannot occupy the same location at all times; in cells, the fastest-ingressing part of the ring travels circumferentially (Figures 1C and S1D). To test whether simulated active gel undergoing speed oscillations recapitulates this phenomenon, we modified our one-dimensional model with periodic boundaries so that the domain was allowed to close. This new model consists of a series of active viscoelastic elements that, arranged in a ring, are pulled inward due to tension. The magnitude of tension is a function of the local concentration of actomyosin-like material. Rings of active gel elements closed asymmetrically, resembling cytokinetic rings *in vivo* (Figures 6A and 6B; Video S4), despite initially uniform activation of the biochemical and mechanical feedback, as is occurring in the *C. elegans* zygote.[65] We also observed the circumferential travel of the region of fastest ingression, as is occurring *in vivo* (Figure 6C). The location of highest material accumulation correlated with the region of fastest ingression, as in cells (Figures 6C and 6D). Also, as in cells, simulated material moved inward radially and did not travel circumferentially (Figure 6A). In sum, these findings support the conclusion that oscillating between activated and dormant states promotes the cytoskeletal remodeling that underlies non-muscle contractility.

DISCUSSION

Here, we report the results of examining a well-studied cell biological subject, the cytokinetic ring of the *C. elegans* zygote, in a new way. By combining unprecedented temporal resolution with observation of the entire ring, rather than an optical section, and by refraining from excessive temporal smoothing or averaging

Please cite this article in press as: Werner et al., Mechanical and biochemical feedback combine to generate complex contractile oscillations in cytokinesis, Current Biology (2024), https://doi.org/10.1016/j.cub.2024.06.037

observations, we discovered a previously unappreciated phenomenon: contractile speed oscillations. Similarly, complex spatiotemporal dynamics are exhibited by a simple model of an active gel controlled by a time-delayed negative feedback loop; when mechanical feedback is added, the system changes from synchronously pulsatile to exhibiting heterogeneous waves.[27] We showed that *in vivo*, as *in silico*, larger mechanical strain leads to longer-period oscillations. When strain is absent or low, contractile oscillations preserve the period of the input biochemical oscillator, RhoA, which we observed to have a pulse timescale of approximately 20 s, shorter than in any other biological context examined. Thus, contractile oscillations emerge from a system of essential, conserved biochemical and structural elements and may be considered inevitable given the biochemical and mechanical feedback intrinsic to the contractile cytoskeleton. In addition, we provide evidence that contractile oscillations may endow the cytoskeleton with functional advantages, by counteracting compaction with remodeling such as polarity sorting, F-actin depolymerization, and unbinding of ring components.

We further developed our active gel model of the contractile ring. Previously, we modeled a one-dimensional domain with fixed periodic boundaries.[27] Here, we extend this work by modeling the active gel on an initially circular ring that shrinks due to contractile stresses. Modeled rings exhibit the oscillatory and spatially asymmetric contraction rates observed in experiments. This allowed us to pose and test hypotheses about the sufficiency of active gel to recapitulate key characteristics of the cytokinetic ring, including ring asymmetry, speed oscillations, and the correlation between contraction speed and material remodeling. Our model was limited to the division plane, omitting the cell poles, which both provide contractile material to the cytokinetic ring[34,35] and resist division plane forces.[58,92] Future modeling efforts will be aided by measuring *in vivo* correlates to the friction within and outside the contractile ring, such as that conferred by crosslinkers including septins (Figure S6), which are not represented in our current model. Future modeling will also take into account the higher dimensionality of the cytokinetic ring *in vivo*, including the two-dimensionality of advective flows, aided by *in vivo* measurements of the correlations among actomyosin flow, furrow constriction, and material remodeling.

Our observations support the hypothesis that cytokinetic rings in animal cells are composed of contractile segments that can contract semi-autonomously.[35,57,73,79,93] This concept synthesizes observations that furrowing speed in some cell types scales with starting ring size,[57,59] that rings repairing after local laser cutting contract faster than uncut rings,[79] and that NMMII organizes in cortical clusters or nodes in *Xenopus* oocytes,[73] *C. elegans* embryos,[60,94] human cells,[55] and *S. pombe*.[95,96] Our ability to resolve foci of ANI-1, a reasonable candidate for a segment marker,[19,52–54,96] suggests that the *C. elegans* zygote ring comprises ~24 initially-4-μm segments. By contrast, the effective length scale of local contractility may be closer to 18 μm, the hydrodynamic length measured in the *C. elegans* zygote during polarization.[97] Despite the possible autonomy of ring segments, the fact that ingression speed is maximal at a single circumferential site at any time point likely relates to the high degree of mechanical coupling among segments via F-actin, cytoskeletal crosslinkers, and scaffolding to the plasma membrane.

While the pulsed nature of RhoA activation is certainly an important driver of speed oscillations, it is likely not sufficient to fully explain them. Indeed, the period of contractile speed oscillations is significantly longer than the timescale of RhoA activity pulses, consistent with the existence of mechanical feedback discussed above. Advection-driven accumulation of passive crosslinkers including anillin will eventually drive the local crosslinker concentration into a regime where contractility is inhibited due to what has been called the "Goldilocks effect," by which force generation is optimal at intermediate concentrations (too little material is incapable of producing force, while too highly concentrated and crosslinked cytoskeleton cannot contract efficiently).[62,84–88] For the cytokinetic ring to maintain high overall ingression speed, other contractile segments must become more contractile as the once-fastest-ingressing segment decelerates, as evidenced by circumferential traveling of the fastest-ingressing segment (Figure 5A). Circumferential travel may be promoted by a pulse of RhoA activity in a nearby region of the ring initiating mechanical feedback. Whether this process is stochastic or influenced by the position of the decelerating ring segment is unclear, since the contractile state of a newly stimulated segment likely influences whether it accelerates.

We have stated that the mechanical feedback in the model implemented here represents advection boosting the local concentration of contractile cytoskeleton.[27] While there is ample precedent for this phenomenon,[33–35,37,52,97] additional mechanical factors could contribute to mechanical feedback. Cortical flows also promote cytoskeletal alignment compatible with contractility.[34,98] The membrane curvature of the furrow may promote circumferential cytoskeletal alignment.[43] F-actin bundling promotes the association of additional binding proteins with the same filament spacing preference.[41,42] Extensile strain on F-actin can change the binding of partners.[99] Compaction can bring a network with suboptimal crosslinking density into a regime more effective at contractility.[87] Stress exerted through catch-bonding myosins prolongs their interaction with F-actin.[44,45] All these phenomena are likely to occur during the remodeling of the non-muscle actomyosin cytoskeleton; their contributions to contractile oscillations may be quantitatively distinguishable. Future work will be aimed at designing assays for local F-actin bundling, order, and strain to test how these other network remodeling events correspond to speed oscillations and how the actomyosin is remodeled during contractility.

Each of the mechanical feedback processes enumerated above has specific molecular mechanisms. The molecules that contribute to these mechanisms have been demonstrated by biophysical assays to bundle, crosslink, mechanosense, and exhibit catch bonding or catch-slip bonding.[1] Conventional cell biological studies, after removing protein function, have defined which proteins are generically necessary for contractility. Our future work will leverage the measurement of contractile speed oscillations to assign specific physical contributions *in vivo*. Testing how such perturbations affect contractile speed oscillations will thus offer novel insight into the mechanical contributions of conserved structural and regulatory ring components.

The high spatial and temporal resolution afforded by simulations (using Cytosim or other approaches) may allow us to test how advective flows and other forms of mechanical feedback correlate with local contractile dynamics of simulated

rings.[58,100,101] We envision that contractile oscillations comprise network compaction (acceleration) and remodeling (deceleration). Correlating contraction speed with cytoskeletal advection, compaction, alignment, and turnover *in silico* and *in vivo* will reveal mechanisms of mechanical feedback. Regardless of the specific aspects of cytoskeletal remodeling that underlie contractile speed oscillations, this novel phenomenon highlights the impacts of coexisting biochemical and mechanical feedback loops and provides unique insights into the dynamics of biological active materials such as the non-muscle actomyosin cytoskeleton.

STAR★METHODS

Detailed methods are provided in the online version of this paper and include the following:

- KEY RESOURCES TABLE
- RESOURCE AVAILABILITY
  - Lead contact
  - Materials availability
  - Data and code availability
- EXPERIMENTAL MODEL AND STUDY PARTICIPANT DETAILS
  - *C. elegans* handling and RNAi
- METHOD DETAILS
  - Live imaging of *C. elegans* embryos
  - Analysis pipeline for 4D image acquisition
  - Quantification of the period of RhoA pulses
  - Calculation of change in fluorescent intensity
  - Quantification of the angle of circumferential travel
  - Active gel model of the actomyosin cortex
  - Simulating pulsatile RhoA activation
  - Modeling the closure dynamics of a contractile ring
  - Figures
- QUANTIFICATION AND STATISTICAL ANALYSIS

SUPPLEMENTAL INFORMATION

Supplemental information can be found online at https://doi.org/10.1016/j.cub.2024.06.037.

ACKNOWLEDGMENTS

The authors are grateful to Ingrid Daubeschies, Hau-Tieng Wu, Ty Hedrick, and J. Steve Marron for their guidance with signal analysis; Paul S. Maddox and the members of both Maddox labs for valuable discussion; and many other members of our mathematics, physics, and cell biology communities for their insights on this project. This work was supported by the National Institute of Health under award no. 1R35GM144238 to A.S.M. and National Science Foundation under award no. NSF MCB-2203601 to S.B.

AUTHOR CONTRIBUTIONS

Conceptualization, M.E.W., A.S.M., M.F.S., and S.B.; methodology, M.E.W., A.S.M., D.D.R., C.B., M.F.S., and S.B.; software, M.E.W., D.D.R., C.B., M.F.S., and F.J.; formal analysis, M.E.W.; investigation, M.E.W.; data curation, M.E.W., D.D.R., and C.B.; writing – original draft, M.E.W. and A.S.M.; writing – review & editing, M.E.W., A.S.M., M.F.S., and S.B.; visualization, M.E.W. and A.S.M.; funding acquisition, A.S.M. and S.B.

DECLARATION OF INTERESTS

The authors declare no competing interests.

Received: December 8, 2023
Revised: April 22, 2024
Accepted: June 13, 2024
Published: July 10, 2024

REFERENCES

1. Banerjee, S., Gardel, M.L., and Schwarz, U.S. (2020). The Actin Cytoskeleton as an Active Adaptive Material. Annu. Rev. Condens. Matter Phys. *11*, 421–439. https://doi.org/10.1146/annurev-conmatphys-031218-013231.
2. Bement, W.M., Leda, M., Moe, A.M., Kita, A.M., Larson, M.E., Golding, A.E., Pfeuti, C., Su, K.C., Miller, A.L., Goryachev, A.B., et al. (2015). Activator-inhibitor coupling between Rho signalling and actin assembly makes the cell cortex an excitable medium. Nat. Cell Biol. *17*, 1471–1483. https://doi.org/10.1038/ncb3251.
3. Zhang, D., and Glotzer, M. (2015). The RhoGAP activity of CYK-4/MgcRacGAP functions non-canonically by promoting RhoA activation during cytokinesis. eLife *4*, e08898. https://doi.org/10.7554/eLife.08898.
4. Graessl, M., Koch, J., Calderon, A., Kamps, D., Banerjee, S., Mazel, T., Schulze, N., Jungkurth, J.K., Patwardhan, R., Solouk, D., et al. (2017). An excitable Rho GTPase signaling network generates dynamic subcellular contraction patterns. J. Cell Biol. *216*, 4271–4285. https://doi.org/10.1083/jcb.201706052.
5. Munjal, A., Philippe, J.M., Munro, E., and Lecuit, T. (2015). A self-organized biomechanical network drives shape changes during tissue morphogenesis. Nature *524*, 351–355. https://doi.org/10.1038/nature14603.
6. Maddox, A.S., Habermann, B., Desai, A., and Oegema, K. (2005). Distinct roles for two C. elegans anillins in the gonad and early embryo. Development *132*, 2837–2848. https://doi.org/10.1242/dev.01828.
7. Hickson, G.R.X., and O'Farrell, P.H. (2008). Rho-dependent control of anillin behavior during cytokinesis. J. Cell Biol. *180*, 285–294. https://doi.org/10.1083/jcb.200709005.
8. Piekny, A.J., and Glotzer, M. (2008). Anillin is a scaffold protein that links RhoA, actin, and myosin during cytokinesis. Curr. Biol. *18*, 30–36. https://doi.org/10.1016/j.cub.2007.11.068.
9. Piekny, A.J., and Maddox, A.S. (2010). The myriad roles of Anillin during cytokinesis. Semin. Cell Dev. Biol. *21*, 881–891. https://doi.org/10.1016/j.semcdb.2010.08.002.
10. Carim, S.C., and Hickson, G.R.X. (2023). The Rho1 GTPase controls anillo-septin assembly to facilitate contractile ring closure during cytokinesis. iScience *26*, 106903. https://doi.org/10.1016/j.isci.2023.106903.
11. Oegema, K., Savoian, M.S., Mitchison, T.J., and Field, C.M. (2000). Functional analysis of a human homologue of the Drosophila actin binding protein anillin suggests a role in cytokinesis. J. Cell Biol. *150*, 539–552. https://doi.org/10.1083/jcb.150.3.539.
12. Pollard, T.D., and O'Shaughnessy, B. (2019). Molecular Mechanism of Cytokinesis. Annu. Rev. Biochem. *88*, 661–689. https://doi.org/10.1146/annurev-biochem-062917-012530.
13. Michaud, A., Swider, Z.T., Landino, J., Leda, M., Miller, A.L., von Dassow, G., Goryachev, A.B., and Bement, W.M. (2021). Cortical excitability and cell division. Curr. Biol. *31*, R553–R559. https://doi.org/10.1016/j.cub.2021.02.053.
14. Fletcher, D.A., and Mullins, R.D. (2010). Cell mechanics and the cytoskeleton. Nature *463*, 485–492. https://doi.org/10.1038/nature08908.
15. Salbreux, G., Charras, G., and Paluch, E. (2012). Actin cortex mechanics and cellular morphogenesis. Trends Cell Biol. *22*, 536–545. https://doi.org/10.1016/j.tcb.2012.07.001.
16. Murrell, M., Oakes, P.W., Lenz, M., and Gardel, M.L. (2015). Forcing cells into shape: the mechanics of actomyosin contractility. Nat. Rev. Mol. Cell Biol. *16*, 486–498. https://doi.org/10.1038/nrm4012.
17. Pollard T.D., O'Shaughnessy B. Molecular mechanism of cytokinesis. Annu Rev Biochem. 2019; 88:661-689. doi: 10/1146/annurev-biochem-062917-012530.

18. Goryachev, A.B., Leda, M., Miller, A.L., von Dassow, G., and Bement, W.M. (2016). How to make a static cytokinetic furrow out of traveling excitable waves. Small GTPases *7*, 65–70. https://doi.org/10.1080/21541248.2016.1168505.

19. Michaux, J.B., Robin, F.B., McFadden, W.M., and Munro, E.M. (2018). Excitable RhoA dynamics drive pulsed contractions in the early C. elegans embryo. J. Cell Biol. *217*, 4230–4252. https://doi.org/10.1083/jcb.201806161.

20. Kamps, D., Koch, J., Juma, V.O., Campillo-Funollet, E., Graessl, M., Banerjee, S., Mazel, T., Chen, X., Wu, Y.W., Portet, S., et al. (2020). Optogenetic Tuning Reveals Rho Amplification-Dependent Dynamics of a Cell Contraction Signal Network. Cell Rep. *33*, 108467. https://doi.org/10.1016/j.celrep.2020.108467.

21. Michaud, A., Leda, M., Swider, Z.T., Kim, S., He, J., Landino, J., Valley, J.R., Huisken, J., Goryachev, A.B., von Dassow, G., et al. (2022). A versatile cortical pattern-forming circuit based on Rho, F-actin, Ect2, and RGA-3/4. J. Cell Biol. *221*, e202203017. https://doi.org/10.1083/jcb.202203017.

22. Bell, K.R., Werner, M.E., Doshi, A., Cortes, D.B., Sattler, A., Vuong-Brender, T., Labouesse, M., and Maddox, A.S. (2020). Novel cytokinetic ring components drive negative feedback in cortical contractility. Mol. Biol. Cell *31*, 1623–1636. https://doi.org/10.1091/mbc.E20-05-0304.

23. Bischof, J., Brand, C.A., Somogyi, K., Májer, I., Thome, S., Mori, M., Schwarz, U.S., and Lénárt, P. (2017). A cdk1 gradient guides surface contraction waves in oocytes. Nat. Commun. *8*, 849. https://doi.org/10.1038/s41467-017-00979-6.

24. Howell, A.S., Jin, M., Wu, C.F., Zyla, T.R., Elston, T.C., and Lew, D.J. (2012). Negative feedback enhances robustness in the yeast polarity establishment circuit. Cell *149*, 322–333. https://doi.org/10.1016/j.cell.2012.03.012.

25. Allard, J., and Mogilner, A. (2013). Traveling waves in actin dynamics and cell motility. Curr. Opin. Cell Biol. *25*, 107–115. https://doi.org/10.1016/j.ceb.2012.08.012.

26. Landino, J., Leda, M., Michaud, A., Swider, Z.T., Prom, M., Field, C.M., Bement, W.M., Vecchiarelli, A.G., Goryachev, A.B., and Miller, A.L. (2021). Rho and F-actin self-organize within an artificial cell cortex. Curr. Biol. *31*, 5613–5621.e5. https://doi.org/10.1016/j.cub.2021.10.021.

27. Staddon, M.F., Munro, E.M., and Banerjee, S. (2022). Pulsatile contractions and pattern formation in excitable actomyosin cortex. PLoS Comput. Biol. *18*, e1009981. https://doi.org/10.1371/journal.pcbi.1009981.

28. Moore, A.S., Coscia, S.M., Simpson, C.L., Ortega, F.E., Wait, E.C., Heddleston, J.M., Nirschl, J.J., Obara, C.J., Guedes-Dias, P., Boecker, C.A., et al. (2021). Actin cables and comet tails organize mitochondrial networks in mitosis. Nature *591*, 659–664. https://doi.org/10.1038/s41586-021-03309-5.

29. Miller, A.L., and Bement, W.M. (2009). Regulation of cytokinesis by Rho GTPase flux. Nat. Cell Biol. *11*, 71–77. https://doi.org/10.1038/ncb1814.

30. Das, M., Drake, T., Wiley, D.J., Buchwald, P., Vavylonis, D., and Verde, F. (2012). Oscillatory dynamics of Cdc42 GTPase in the control of polarized growth. Science *337*, 239–243. https://doi.org/10.1126/science.1218377.

31. Moore, A.S., Wong, Y.C., Simpson, C.L., and Holzbaur, E.L.F. (2016). Dynamic actin cycling through mitochondrial subpopulations locally regulates the fission-fusion balance within mitochondrial networks. Nat. Commun. *7*, 12886. https://doi.org/10.1038/ncomms12886.

32. Xiao, S., Tong, C., Yang, Y., and Wu, M. (2017). Mitotic Cortical Waves Predict Future Division Sites by Encoding Positional and Size Information. Dev. Cell *43*, 493–506.e3. https://doi.org/10.1016/j.devcel.2017.10.023.

33. White, J.G., and Borisy, G.G. (1983). On the mechanisms of cytokinesis in animal cells. J. Theor. Biol. *101*, 289–316. https://doi.org/10.1016/0022-5193(83)90342-9.

34. Reymann, A.C., Staniscia, F., Erzberger, A., Salbreux, G., and Grill, S.W. (2016). Cortical flow aligns actin filaments to form a furrow. eLife *5*, 1–25. https://doi.org/10.7554/eLife.17807.

35. Khaliullin, R.N., Green, R.A., Shi, L.Z., Gomez-Cavazos, J.S., Berns, M.W., Desai, A., and Oegema, K. (2018). A positive-feedback-based mechanism for constriction rate acceleration during cytokinesis in Caenorhabditis elegans. eLife *7*, e36073. https://doi.org/10.7554/eLife.36073.

36. Salbreux, G., Prost, J., and Joanny, J.F. (2009). Hydrodynamics of cellular cortical flows and the formation of contractile rings. Phys. Rev. Lett. *103*, 058102. https://doi.org/10.1103/PhysRevLett.103.058102.

37. Nishikawa, M., Naganathan, S.R., Jülicher, F., and Grill, S.W. (2017). Controlling contractile instabilities in the actomyosin cortex. eLife *6*, e19595. https://doi.org/10.7554/eLife.19595.

38. Li, Y., and Munro, E. (2021). Filament-guided filament assembly provides structural memory of filament alignment during cytokinesis. Dev. Cell *56*, 2486–2500.e6. https://doi.org/10.1016/j.devcel.2021.08.009.

39. Yao, B., Donoughe, S., Michaux, J., and Munro, E. (2022). Modulating RhoA effectors induces transitions to oscillatory and more wavelike RhoA dynamics in Caenorhabditis elegans zygotes. Mol. Biol. Cell *33*, ar58. https://doi.org/10.1091/mbc.E21-11-0542.

40. Sherer, L.A., and Courtemanche, N. (2022). Cooperative bundling by fascin generates actin structures with architectures that depend on filament length. Front. Cell Dev. Biol. *10*, 974047. https://doi.org/10.3389/fcell.2022.974047.

41. Winkelman, J.D., Suarez, C., Hocky, G.M., Harker, A.J., Morganthaler, A.N., Christensen, J.R., Voth, G.A., Bartles, J.R., and Kovar, D.R. (2016). Fascin- and alpha-Actinin-Bundled Networks Contain Intrinsic Structural Features that Drive Protein Sorting. Curr. Biol. *26*, 2697–2706. https://doi.org/10.1016/j.cub.2016.07.080.

42. Christensen, J.R., Homa, K.E., Morganthaler, A.N., Brown, R.R., Suarez, C., Harker, A.J., O'Connell, M.E., and Kovar, D.R. (2019). Cooperation between tropomyosin and alpha-actinin inhibits fimbrin association with actin filament networks in fission yeast. eLife *8*, e47279. https://doi.org/10.7554/eLife.47279.

43. Dorn, J.F., Zhang, L., Phi, T.-T., Lacroix, B., Maddox, P.S., Liu, J., and Maddox, A.S. (2016). A theoretical model of cytokinesis implicates feedback between membrane curvature and cytoskeletal organization in asymmetric cytokinetic furrowing. Mol. Biol. Cell *27*, 1286–1299. https://doi.org/10.1091/mbc.E15-06-0374.

44. Cortes, D.B., Gordon, M., Nédélec, F., and Maddox, A.S. (2020). Bond Type and Discretization of Nonmuscle Myosin II Are Critical for Simulated Contractile Dynamics. Biophys. J. *118*, 2703–2717. https://doi.org/10.1016/j.bpj.2020.03.033.

45. Coluccio, L.M., and Geeves, M.A. (1999). Transient kinetic analysis of the 130-kDa myosin I (MYR-1 gene product) from rat liver. A myosin I designed for maintenance of tension? J. Biol. Chem. *274*, 21575–21580. https://doi.org/10.1074/jbc.274.31.21575.

46. Erdmann, T., Albert, P.J., and Schwarz, U.S. (2013). Stochastic dynamics of small ensembles of non-processive molecular motors: The parallel cluster model. J. Chem. Phys. *139*, 175104. https://doi.org/10.1063/1.4827497.

47. Guo, B., and Guilford, W.H. (2006). Mechanics of actomyosin bonds in different nucleotide states are tuned to muscle contraction. Proc. Natl. Acad. Sci. USA *103*, 9844–9849. https://doi.org/10.1073/pnas.0601255103.

48. Stam, S., Alberts, J., Gardel, M.L., and Munro, E. (2015). Isoforms confer characteristic force generation and mechanosensation by myosin II filaments. Biophys. J. *108*, 1997–2006. https://doi.org/10.1016/j.bpj.2015.03.030.

49. Nishizaka, T., Miyata, H., Yoshikawa, H., Ishiwata, S., and Kinosita, K., Jr. (1995). Unbinding force of a single motor molecule of muscle measured using optical tweezers. Nature *377*, 251–254. https://doi.org/10.1038/377251a0.

50. Yamada, A., Mamane, A., Lee-Tin-Wah, J., Di Cicco, A., Prévost, C., Lévy, D., Joanny, J.F., Coudrier, E., and Bassereau, P. (2014). Catch-bond behaviour facilitates membrane tubulation by non-processive myosin 1b. Nat. Commun. *5*, 3624. https://doi.org/10.1038/ncomms4624.

51. Basant, A., and Glotzer, M. (2018). Spatiotemporal Regulation of RhoA during Cytokinesis. Curr. Biol. *28*, R570–R580. https://doi.org/10.1016/j.cub.2018.03.045.

52. Robin, F.B., McFadden, W.M., Yao, B., and Munro, E.M. (2014). Single-molecule analysis of cell surface dynamics in Caenorhabditis elegans embryos. Nat. Methods *11*, 677–682. https://doi.org/10.1038/nmeth.2928.

53. Pollard, T.D., and Wu, J.Q. (2010). Understanding cytokinesis: lessons from fission yeast. Nat. Rev. Mol. Cell Biol. *11*, 149–155. https://doi.org/10.1038/nrm2834.

54. Mayer, M., Depken, M., Bois, J.S., Jülicher, F., and Grill, S.W. (2010). Anisotropies in cortical tension reveal the physical basis of polarizing cortical flows. Nature *467*, 617–621. https://doi.org/10.1038/nature09376.

55. Wollrab, V., Thiagarajan, R., Wald, A., Kruse, K., and Riveline, D. (2016). Still and rotating myosin clusters determine cytokinetic ring constriction. Nat. Commun. *7*, 11860. https://doi.org/10.1038/ncomms11860.

56. Huang, J., Chew, T.G., Gu, Y., Palani, S., Kamnev, A., Martin, D.S., Carter, N.J., Cross, R.A., Oliferenko, S., and Balasubramanian, M.K. (2016). Curvature-induced expulsion of actomyosin bundles during cytokinetic ring contraction. eLife *5*, e21383. https://doi.org/10.7554/eLife.21383.

57. Carvalho, A., Desai, A., and Oegema, K. (2009). Structural Memory in the Contractile Ring Makes the Duration of Cytokinesis Independent of Cell Size. Cell *137*, 926–937. https://doi.org/10.1016/j.cell.2009.03.021.

58. Cortes, D.B., Maddox, P.S., Nédéléç, F.J., and Maddox, A.S. (2023). Contractile ring composition dictates kinetics of in silico contractility. Biophys. J. *122*, 3611–3629. https://doi.org/10.1016/j.bpj.2022.12.026.

59. Calvert, M.E.K., Wright, G.D., Leong, F.Y., Chiam, K.H., Chen, Y., Jedd, G., and Balasubramanian, M.K. (2011). Myosin concentration underlies cell size-dependent scalability of actomyosin ring constriction. J. Cell Biol. *195*, 799–813. https://doi.org/10.1083/jcb.201101055.

60. Munro, E., Nance, J., and Priess, J.R. (2004). Cortical flows powered by asymmetrical contraction transport PAR proteins to establish and maintain anterior-posterior polarity in the early C. elegans embryo. Dev. Cell *7*, 413–424. https://doi.org/10.1016/j.devcel.2004.08.001.

61. Martin, A.C., Kaschube, M., and Wieschaus, E.F. (2009). Pulsed contractions of an actin-myosin network drive apical constriction. Nature *457*, 495–499. https://doi.org/10.1038/nature07522.

62. Belmonte, J.M., Leptin, M., and Nédélec, F. (2017). A theory that predicts behaviors of disordered cytoskeletal networks. Mol. Syst. Biol. *13*, 941. https://doi.org/10.15252/msb.20177796.

63. Krishna, A., Savinov, M., Ierushalmi, N., Mogilner, A., and Keren, K. (2024). Size-dependent transition from steady contraction to waves in actomyosin networks with turnover. Nat. Phys. *20*, 123–134. https://doi.org/10.1038/s41567-023-02271-5.

64. Bourdages, K.G., Lacroix, B., Dorn, J.F., Descovich, C.P., and Maddox, A.S. (2014). Quantitative analysis of cytokinesis in situ during C. elegans postembryonic development. PLoS One *9*, e110689. https://doi.org/10.1371/journal.pone.0110689.

65. Maddox, A.S., Lewellyn, L., Desai, A., and Oegema, K. (2007). Anillin and the septins promote asymmetric ingression of the cytokinetic furrow. Dev. Cell *12*, 827–835. https://doi.org/10.1016/j.devcel.2007.02.018.

66. Audhya, A., Hyndman, F., McLeod, I.X., Maddox, A.S., Yates, J.R., 3rd, Desai, A., and Oegema, K. (2005). A complex containing the Sm protein CAR-1 and the RNA helicase CGH-1 is required for embryonic cytokinesis in Caenorhabditis elegans. J. Cell Biol. *171*, 267–279. https://doi.org/10.1083/jcb.200506124.

67. Rehain-Bell, K., Love, A., Werner, M.E., MacLeod, I., Yates, J.R., 3rd, and Maddox, A.S. (2017). A Sterile 20 Family Kinase and Its Co-factor CCM-3 Regulate Contractile Ring Proteins on Germline Intercellular Bridges. Curr. Biol. *27*, 860–867. https://doi.org/10.1016/j.cub.2017.01.058.

68. Singh, D., Odedra, D., Dutta, P., and Pohl, C. (2019). Mechanical stress induces a scalable switch in cortical flow polarization during cytokinesis. J. Cell Sci. *132*, https://doi.org/10.1242/jcs.231357.

69. Rappaport, R. (1996). Cytokinesis in Animal Cells (Cambridge University Press).

70. Singh, D., and Pohl, C. (2014). Coupling of rotational cortical flow, asymmetric midbody positioning, and spindle rotation mediates dorsoventral axis formation in C. elegans. Dev. Cell *28*, 253–267. https://doi.org/10.1016/j.devcel.2014.01.002.

71. Schonegg, S., Hyman, A.A., and Wood, W.B. (2014). Timing and mechanism of the initial cue establishing handed left-right asymmetry in Caenorhabditis elegans embryos. Genesis *52*, 572–580. https://doi.org/10.1002/dvg.22749.

72. Zaatri, A., Perry, J.A., and Maddox, A.S. (2021). Septins and a formin have distinct functions in anaphase chiral cortical rotation in the Caenorhabditis elegans zygote. Mol. Biol. Cell *32*, 1283–1292. https://doi.org/10.1091/mbc.E20-09-0576.

73. Bement, W.M., and Capco, D.G. (1991). Analysis of Inducible Contractile Rings Suggests a Role for Protein Kinase C in Embryonic Cytokinesis and Wound Healing. Cell Motil. Cytoskeleton *20*, 145–157. https://doi.org/10.1002/cm.970200207.

74. Daubechies, I., Lu, J., and Wu, H.-T. (2011). Synchrosqueezed wavelet transforms: An empirical mode decomposition-like tool. Appl. Comp. Harmon. Anal. *30*, 243–261. https://doi.org/10.1016/j.acha.2010.08.002.

75. Thakur, G., Brevdo, E., Fučkar, N.S., and Wu, H.-T. (2013). The Synchrosqueezing algorithm for time-varying spectral analysis: robustness properties and new paleoclimate applications. Signal Process. *93*, 1079–1094. https://doi.org/10.1016/j.sigpro.2012.11.029.

76. Lin, C.-Y., Su, L., and Wu, H.-T. (2018). Wave-Shape Function Analysis. J. Fourier Anal. Appl. *24*, 451–505. https://doi.org/10.1007/s00041-017-9523-0.

77. Linsmeier, I., Banerjee, S., Oakes, P.W., Jung, W., Kim, T., and Murrell, M.P. (2016). Disordered actomyosin networks are sufficient to produce cooperative and telescopic contractility. Nat. Commun. *7*, 12615. https://doi.org/10.1038/ncomms12615.

78. Piekny, A.J., and Mains, P.E. (2002). Rho-binding kinase (LET-502) and myosin phosphatase (MEL-11) regulate cytokinesis in the early Caenorhabditis elegans embryo. J. Cell Sci. *115*, 2271–2282. https://doi.org/10.1242/jcs.115.11.2271.

79. Silva, A.M., Osório, D.S., Pereira, A.J., Maiato, H., Pinto, I.M., Rubinstein, B., Gassmann, R., Telley, I.A., and Carvalho, A.X. (2016). Robust gap repair in the contractile ring ensures timely completion of cytokinesis. J. Cell Biol. *215*, 789–799. https://doi.org/10.1083/jcb.201605080.

80. Lewellyn, L., Dumont, J., Desai, A., and Oegema, K. (2010). Analyzing the effects of delaying aster separation on furrow formation during cytokinesis in the Caenorhabditis elegans embryo. Mol. Biol. Cell *21*, 50–62. https://doi.org/10.1091/mbc.e09-01-0089.

81. Swider, Z.T., Michaud, A., Leda, M., Landino, J., Goryachev, A.B., and Bement, W.M. (2022). Cell cycle and developmental control of cortical excitability in Xenopus laevis. Mol. Biol. Cell *33*, ar73. https://doi.org/10.1091/mbc.E22-01-0025.

82. Tse, Y.C., Werner, M., Longhini, K.M., Labbe, J.C., Goldstein, B., and Glotzer, M. (2012). RhoA activation during polarization and cytokinesis of the early Caenorhabditis elegans embryo is differentially dependent on NOP-1 and CYK-4. Mol. Biol. Cell *23*, 4020–4031. https://doi.org/10.1091/mbc.E12-04-0268.

83. Zhuravlev, Y., Hirsch, S.M., Jordan, S.N., Dumont, J., Shirasu-Hiza, M., and Canman, J.C. (2017). CYK-4 regulates Rac, but not Rho, during cytokinesis. Mol. Biol. Cell *28*, 1258–1270. https://doi.org/10.1091/mbc.E17-01-0020.

84. Li, Y., Christensen, J.R., Homa, K.E., Hocky, G.M., Fok, A., Sees, J.A., Voth, G.A., and Kovar, D.R. (2016). The F-actin bundler alpha-actinin Ain1 is tailored for ring assembly and constriction during cytokinesis in fission yeast. Mol. Biol. Cell *27*, 1821–1833. https://doi.org/10.1091/mbc.E16-01-0010.

85. Descovich, C.P., Cortes, D.B., Ryan, S., Nash, J., Zhang, L., Maddox, P.S., Nedelec, F., and Maddox, A.S. (2018). Cross-linkers both drive and brake cytoskeletal remodeling and furrowing in cytokinesis. Mol. Biol. Cell *29*, 622–631. https://doi.org/10.1091/mbc.E17-06-0392.

86. Ding, W.Y., Ong, H.T., Hara, Y., Wongsantichon, J., Toyama, Y., Robinson, R.C., Nédélec, F., and Zaidel-Bar, R. (2017). Plastin increases cortical connectivity to facilitate robust polarization and timely cytokinesis. J. Cell Biol. *216*, 1371–1386. https://doi.org/10.1083/jcb.201603070.

87. Ennomani, H., Letort, G., Guérin, C., Martiel, J.L., Cao, W., Nédélec, F., De La Cruz, E.M., Théry, M., and Blanchoin, L. (2016). Architecture and Connectivity Govern Actin Network Contractility. Curr. Biol. *26*, 616–626. https://doi.org/10.1016/j.cub.2015.12.069.

88. Mukhina, S., Wang, Y.L., and Murata-Hori, M. (2007). Alpha-actinin is required for tightly regulated remodeling of the actin cortical network during cytokinesis. Dev. Cell *13*, 554–565. https://doi.org/10.1016/j.devcel.2007.08.003.

89. Lenz, M., Thoresen, T., Gardel, M.L., and Dinner, A.R. (2012). Contractile Units in Disordered Actomyosin Bundles Arise from F-Actin Buckling. Phys. Rev. Lett. *108*, 238107. https://doi.org/10.1103/PhysRevLett.108.238107.

90. Murrell, M.P., and Gardel, M.L. (2012). F-actin buckling coordinates contractility and severing in a biomimetic actomyosin cortex. In Proceedings of the National Academy of Sciences.

91. Weirich, K.L., Stam, S., Munro, E., and Gardel, M.L. (2021). Actin bundle architecture and mechanics regulate myosin II force generation. Biophys. J. *120*, 1957–1970. https://doi.org/10.1016/j.bpj.2021.03.026.

92. Turlier, H., Audoly, B., Prost, J., and Joanny, J.F. (2014). Furrow Constriction in Animal Cell Cytokinesis. Biophys. J. *106*, 114–123. https://doi.org/10.1016/j.bpj.2013.11.014.

93. Savoian, M.S., Khodjakov, A., and Rieder, C.L. (1999). Unilateral and wandering furrows during mitosis in vertebrates: implications for the mechanism of cytokinesis. Cell Biol. Int. *23*, 805–812. https://doi.org/10.1006/cbir.1999.0477.

94. Werner, M., Munro, E., and Glotzer, M. (2007). Astral Signals Spatially Bias Cortical Myosin Recruitment to Break Symmetry and Promote Cytokinesis. Curr. Biol. *17*, 1286–1297. https://doi.org/10.1016/j.cub.2007.06.070.

95. Paoletti, A., and Chang, F. (2000). Analysis of mid1p, a protein required for placement of the cell division site, reveals a link between the nucleus and the cell surface in fission yeast. Mol. Biol. Cell *11*, 2757–2773. https://doi.org/10.1091/mbc.11.8.2757.

96. Mangione, M.C., and Gould, K.L. (2019). Molecular form and function of the cytokinetic ring. J. Cell Sci. *132*, jcs226928. https://doi.org/10.1242/jcs.226928.

97. Naganathan, S.R., Fürthauer, S., Rodriguez, J., Fievet, B.T., Jülicher, F., Ahringer, J., Cannistraci, C.V., and Grill, S.W. (2018). Morphogenetic degeneracies in the actomyosin cortex. eLife *7*, e37677. https://doi.org/10.7554/eLife.37677.

98. Zumdieck, A., Kruse, K., Bringmann, H., Hyman, A.A., and Jülicher, F. (2007). Stress generation and filament turnover during actin ring constriction. PLoS One *2*, e696. https://doi.org/10.1371/journal.pone.0000696.

99. Zimmermann, D., Homa, K.E., Hocky, G.M., Pollard, L.W., De La Cruz, E.M., Voth, G.A., Trybus, K.M., and Kovar, D.R. (2017). Mechanoregulated inhibition of formin facilitates contractile actomyosin ring assembly. Nat. Commun. *8*, 703. https://doi.org/10.1038/s41467-017-00445-3.

100. Cortes, D.B., Dawes, A., Liu, J., Nickaeen, M., Strychalski, W., and Maddox, A.S. (2018). Unite to divide - how models and biological experimentation have come together to reveal mechanisms of cytokinesis. J. Cell Sci. *131*, jcs203570. https://doi.org/10.1242/jcs.203570.

101. Vavylonis, D., Wu, J.Q., Hao, S., O'Shaughnessy, B., and Pollard, T.D. (2008). Assembly mechanism of the contractile ring for cytokinesis by fission yeast. Science *319*, 97–100. https://doi.org/10.1126/science.1151086.

102. Dickinson, D.J., Ward, J.D., Reiner, D.J., and Goldstein, B. (2013). Engineering the Caenorhabditis elegans genome using Cas9-triggered homologous recombination. Nat. Methods *10*, 1028–1034. https://doi.org/10.1038/nmeth.2641.

103. Schindelin, J., Arganda-Carreras, I., Frise, E., Kaynig, V., Longair, M., Pietzsch, T., Preibisch, S., Rueden, C., Saalfeld, S., Schmid, B., et al. (2012). Fiji: an open-source platform for biological-image analysis. Nat. Methods *9*, 676–682. https://doi.org/10.1038/nmeth.2019.

104. Tinevez, J.Y., Perry, N., Schindelin, J., Hoopes, G.M., Reynolds, G.D., Laplantine, E., Bednarek, S.Y., Shorte, S.L., and Eliceiri, K.W. (2017). TrackMate: An open and extensible platform for single-particle tracking. Methods *115*, 80–90. https://doi.org/10.1016/j.ymeth.2016.09.016.

105. Brenner, S. (1974). The genetics of Caenorhabditis elegans. Genetics *77*, 71–94. https://doi.org/10.1093/genetics/77.1.71.

106. Kamath, R.S., and Ahringer, J. (2003). Genome-wide RNAi screening in Caenorhabditis elegans. Methods *30*, 313–321. https://doi.org/10.1016/s1046-2023(03)00050-1.

107. Kamath, R.S., Fraser, A.G., Dong, Y., Poulin, G., Durbin, R., Gotta, M., Kanapin, A., Le Bot, N., Moreno, S., Sohrmann, M., et al. (2003). Systematic functional analysis of the Caenorhabditis elegans genome using RNAi. Nature *421*, 231–237. https://doi.org/10.1038/nature01278.

108. Schneider, C.A., Rasband, W.S., and Eliceiri, K.W. (2012). NIH Image to ImageJ: 25 years of image analysis. Nat. Methods *9*, 671–675. https://doi.org/10.1038/nmeth.2089.

109. Rueden, C.T., Schindelin, J., Hiner, M.C., DeZonia, B.E., Walter, A.E., Arena, E.T., and Eliceiri, K.W. (2017). ImageJ2: ImageJ for the next generation of scientific image data. BMC Bioinformatics *18*, 529. https://doi.org/10.1186/s12859-017-1934-z.

110. Holoborodko, P. (2008). Smooth noise-robust differentiators. Pavel Holoborodko Applied mathematics and beyond. http://www.holoborodko.com/pavel/numerical-methods/numerical-derivative/smooth-low-noise-differentiators/.

111. Suzen, M. (2023). Generate Weighted Histogram (MATLAB Central File Exchange). https://www.mathworks.com/matlabcentral/fileexchange/42493-generate-weighted-histogram.

112. Saha, A., Nishikawa, M., Behrndt, M., Heisenberg, C.P., Jülicher, F., and Grill, S.W. (2016). Determining Physical Properties of the Cell Cortex. Biophys. J. *110*, 1421–1429. https://doi.org/10.1016/j.bpj.2016.02.013.

113. Guyer, J.E., Wheeler, D., and Warren, J.A. (2009). FiPy: Partial Differential Equations with Python. Comput. Sci. Eng. *11*, 6–15. https://doi.org/10.1109/MCSE.2009.52.

114. Jonas. (2023). plot spread points (beeswarm plot) (MATLAB Central File Exchange). https://www.mathworks.com/matlabcentral/fileexchange/37105-plot-spread-points-beeswarm-plot.

Please cite this article in press as: Werner et al., Mechanical and biochemical feedback combine to generate complex contractile oscillations in cytokinesis, Current Biology (2024), https://doi.org/10.1016/j.cub.2024.06.037

STAR★METHODS

KEY RESOURCES TABLE

REAGENT or RESOURCE	SOURCE	IDENTIFIER
Experimental models: Organisms/strains		
C. elegans strain: EM328; genotype: *let-502(mc74 [GFP::let-502])I; (zuIs151 [nmy-2::NMY-2-mRFP; unc-119(+)])*	Bell et al.[22]	N/A
C. elegans strain: LP162; genotype: *cp13[nmy-2::gfp + LoxP]) I.*	Dickinson et al.[102]	N/A
C. elegans strain: MDX40; genotype: *nmy-2(cp52[nmy-2::mkate2 + LoxP unc-119(+) LoxP]) I; ani-1(mon7[mNeonGreen^3xFlag::ani-1]) III*	Rehain-Bell et al.[67]	N/A
Software and algorithms		
Fiji	Schindelin et al.[103]	https://imagej.net/downloads
Trackmate	Tinevez et al.[104]	https://imagej.net/plugins/trackmate/
Matlab	Mathworks	https://www.mathworks.com/products/matlab.html
Microsoft Office	Microsoft	
Python	Anaconda	https://www.anaconda.com/products/navigator
Ring segmentation, Mode decomposition, data analysis and mathematical model	This study: Zenodo: https://doi.org/10.5281/zenodo.11478957	Github: https://github.com/michaelewerner/Werner_et.al._submitted_2023

RESOURCE AVAILABILITY

Lead contact

Further information and requests for resources and reagents should be directed to and will be fulfilled by the lead contact, Amy Shaub Maddox (asm@email.unc.edu).

Materials availability

Worm strains used in this study are available upon request from the lead contact.

Data and code availability

- Microscopy data reported in this paper will be shared by the lead contact upon request.
- All original code has been deposited at https://github.com/michaelewerner/Werner_et.al._submitted_2023.git and is publicly available as of the date of publication. DOIs are listed in the key resources table.
- Any additional information required to reanalyze the data reported in this paper is available from the lead contact upon request.

EXPERIMENTAL MODEL AND STUDY PARTICIPANT DETAILS

C. elegans handling and RNAi

Worm strains (see key resources table) were maintained at 20°C as described previously.[105] LP162 was a gift from Dan Dickinson and Bob Goldstein. RNAi was performed by feeding HT115 *E. coli* bacteria expressing double-strand RNA at 20°C as described previously for 24 hours unless specified otherwise.[106,107] For partial *ect-2(RNAi)*, worms were incubated for 20-22 hours at 20°C and only embryos with at least 20% reduction in overall closure time but still completing cytokinesis were used for analysis.

METHOD DETAILS

Live imaging of *C. elegans* embryos

For all experiments except Figures 4B and 4C, embryos were dissected from gravid hermaphrodites into a drop M9 and sealed between a coverslip and slide with VaLaP. For microscopy, chambers were inverted and embryos were imaged freely resting on the

Please cite this article in press as: Werner et al., Mechanical and biochemical feedback combine to generate complex contractile oscillations in cytokinesis, Current Biology (2024), https://doi.org/10.1016/j.cub.2024.06.037

coverslip to avoid compression. For Figures 4B and 4C, gravid hermaphrodites were dissected into M9 and gently compressed between a coverslip and an 2% agar pad.

All acquisition was performed on a Nikon A1R microscope body with a Gallium arsenide phosphide photo-multiplier tube (GaAsP PMT) detector using NIS-elements. A 60 × 1.41 NA Nikon Oil Immersion Objective (Figures 4B and 4C) or a 60 × 1.27 NA Nikon Water Immersion Objective (all other figures) were used for image acquisition. For Figures 4B and 4C, data were acquired from single Z-sections at the embryonic cortex with a sampling frequency of 1 s using the Galvano point scanner. Acquisition for all other figures was performed using the resonance scanner acquiring 40 confocal sections with 1 μm spacing through the entire embryo every 2.7 seconds with a PI (Physik Instruments) 100 μm stage insert Z piezo triggered directly from the A1 confocal controller.

Analysis pipeline for 4D image acquisition

A 10 μm area surrounding the cytokinetic furrow was selected and an end-on reconstruction was created using the Reslice function in ImageJ. The resulting image stack was average-intensity projected into two dimensions.[103,108,109] The resulting tiff stack was segmented using a custom Python script that fits a polygon to the cytokinetic ring based on mNeonGreen::ANI-1 or NMY-2::GFP fluorescence intensity. The resulting polygon was visually verified and divided into 72 equal angular segments and the coordinates for the center of the segment were recorded for each time point. The Fourier coefficients of the resulting coordinates were spatially smoothed by fitting a 2D harmonic series with 3 harmonics and temporally smoothed using a moving average over 5 time points. A smoothed inward velocity of individual segments was derived using a smooth differentiator function described previously.[110] The resulting velocity and acceleration data was further analyzed using custom Matlab scripts. Mode decomposition of the acceleration input signal was performed using the Matlab wavelet synchrosqueeze transform function (WSST) function using Morlet wavelets as a Kernel and 32 voices per octave.[74,75] The 25 highest energy ''ridges'' in the wavelet synchrosqueeze transform matrix that represents the signal were identified using the Wsstridge function in Matlab with a penalty of 2 and 2 frequency bins. Each of these ridges represented a part (or mode) of the signal, which was ultimately reconstructed via addition of the modes. The various mode combinations from the adaptive nonharmonic model were fit to experimental input data. For each cell and spatial segment, we found the representation of that signal as a maximum of 5 simple waves that would reconstruct the input signal with a minimal root-mean-squared error (RMSE). The amplitudes of each mode for the model fit with the lowest RSME was obtained from the Hilbert transform of the corresponding intrinsic mode functions and the mode periods were calculated as the inverse of the frequency output of the WSST. Weighted histograms were created in Matlab by aggregating all mode frequencies from the ANH fit with the lowest RMSE and adjusting the amplitudes by their corresponding angular frequencies and normalizing the data to the frequency bin with the largest amplitude.[111]

Quantification of the period of RhoA pulses

LET-502::GFP foci were identified and tracked using Fiji plug-in TrackMate.[22,104] Analysis of LET-502 foci was performed on single cortical plane images of the first 2 minutes following anaphase onset in a 20 μm region surrounding the presumptive site of furrow ingression. Prior to analysis using TrackMate, single cortical plane images were normalized in Fiji. In TrackMate the LoG detector function with an estimated focus diameter of 3 μm and median filter thresholding was used to detect foci, and the LAP tracer function with ''no gap closing distance'' and maximum linking distance of 2 μm was used to track foci. Processing and analysis of foci properties determined using TrackMate were performed using custom scripts in MATLAB. Pulse periods were also scored manually by visually identifying the first and last frame for at least 5 foci for each scored embryo, resulting in average pulse periods similar to those obtained with the automated tracking approach using Trackmate.

Calculation of change in fluorescent intensity

Using a custom Matlab script, pixels corresponding to the center of the 72 angular segments derived from the segmented polygon described above were identified in the average-intensity projected image stack used for the segmentation. Intensity values for each pixel as well as the 8 pixels surrounding the pixel were extracted and averaged for each segment at each timepoint to obtain a mean intensity value for each segment. Change of intensity for each segment at each timepoint (t) was then determined by subtracting the intensity at timepoint t+1. Intensity values were smoothed by a moving average over 2 timepoints and normalized to the range of intensity changes for each timepoint. For Figures 5D, 5E, S5C, and S5D, the segment with the highest change in intensity of mNeonGreen::ANI-1 or NMY-2::GFP was determined for each time point. The change of fluorescence intensity for up to the 54 seconds (20 timepoints; as available) preceding and following each given timepoint for said segment were determined. Data from each timepoint were aligned in time at the timepoint corresponding to the highest change in intensity, and mean values for each timepoint for individual embryos were calculated. For each of these timepoints, corresponding speed and change of speed values were extracted and averaged.

Quantification of the angle of circumferential travel

The angles between the time axis and the manually assigned vector of displacement in kymographs from intensity or velocity kymographs of the 42 angular segments closest to the coverslip were determined using a custom Matlab script. Resulting absolute angular value distributions were represented in rose plots generated in Matlab. For kymograph analysis, intensity and velocity values for individual segments were range normalized for each time points.

Please cite this article in press as: Werner et al., Mechanical and biochemical feedback combine to generate complex contractile oscillations in cytokinesis, Current Biology (2024), https://doi.org/10.1016/j.cub.2024.06.037

Active gel model of the actomyosin cortex

Active gel model in 1D domain with periodic boundary condition: To simulate actomyosin dynamics within the contractile ring, we adapted our previously published active gel theory of the actomyosin cortex.[27] This model implements a coupled reaction-diffusion system comprising the concentrations of RhoA and actomyosin. This reaction-diffusion system is then coupled to the mechanics of an active contractile gel, representing the actomyosin network in the cortex. As described previously[19] the concentration of RhoA, r, is produced at some basal rate and increases its own production autocatalytically. Actomyosin, with concentration m, locally degrades RhoA at a rate g, resulting in an overall production rate of RhoA:

$$R_r(r,m) = S + \frac{ar}{r_a + r} - \frac{gmr}{r_g + r}. \quad \text{(Equation 1)}$$

In the above equation, it is assumed that the production and degradation terms saturate with RhoA concentration. At the same time, RhoA promotes the assembly of actomyosin at a rate k_a, which then disassembles at a rate k_d, yielding a net production rate of actomyosin:

$$R_m(r,m) = S_m + k_a r^2 - k_d m. \quad \text{(Equation 2)}$$

Furthermore, RhoA and actomyosin can diffuse within the cortex with diffusion constants D_r and D_m, respectively, and be advected with actomyosin flows on the cortical surface. Thus, the equations describing the spatiotemporal dynamics of RhoA and actomyosin concentrations are given by:

$$\dot{r} + \partial_x(rv) = R_r(r,m) + D_r\partial_x^2 r \quad \text{(Equation 3)}$$

$$\dot{m} + \partial_x(mv) = R_m(r,m) + D_m\partial_x^2 m \quad \text{(Equation 4)}$$

where dot denotes time derivative and v is the velocity of actomyosin flow. The second terms in the left-hand side of the above equations represent advection with actomyosin flows and the last terms in the right-hand side represent diffusion.

We model the actomyosin cortex as a 1-dimensional active Maxwell viscoelastic material, which behaves like a fluid at long times (due to turnover), with active stress generated by the actomyosin. The equation of motion is given by:

$$\gamma(v + \tau\dot{v}) = \eta\,\partial_x^2 v + \sigma_a\partial_x\left(\frac{m}{m_0 + m}\right) \quad \text{(Equation 5)}$$

where $v$is the velocity of the cortex, γ is the friction between the cortex and the cytosol, η is the viscosity of the cortex, σ_a is the maximum active stress magnitude, with the last term representing active contraction by actomyosin which saturates at high concentrations ($m \gg m_0$).[77]

The default parameters were obtained from experimental data.[19] Parameters for active stress and mechanical properties of the cortex are taken from Saha et al.[112] The diffusion rates for RhoA and actomyosin are taken from Nishikawa et al.[37] We simulated the model by numerically integrating the equations using the fipy package in python,[113] using a 1-dimentional periodic box of length 140 μm.

Default biochemical parameters	Value
S_r	0.01 s^{-}·
A	0.1609 s^{-}·
N	1
r_a	0.3833
G	0.1787 s^{-}·
r_g	0.01
S_m	0.0076 s^{-}·
k_a	0.1408 s^{-}·
k_d	0.0828 s^{-}·
D_r	0.1 $\mu m^2 s^{-}$·
D_m	0.01 $\mu m^2 s^{-}$·
γ_t	1 Ns^{-} μm^2
γ_n	10 Ns^{-0} μm^2
T	5s
Λ	14.3 μm
σ_a/γ	49.8 $\mu m^2 s^{-9}$

Please cite this article in press as: Werner et al., Mechanical and biochemical feedback combine to generate complex contractile oscillations in cytokinesis, Current Biology (2024), https://doi.org/10.1016/j.cub.2024.06.037

The period of generated pulsatile contractions was measured using a Fourier transform of the actomyosin field at each segment of the cortex for the final 500 seconds of each simulation. The frequency power for each simulation was obtained by averaging the Fourier transform output over all spatial dimensions.

Simulating pulsatile RhoA activation

To apply a pulsatile stimulus with a period of 20 seconds to the excitable one-dimensional cortex, a pulsatile stimulus was simulated as the product of the positive values of 2 phase shifted sine waves with a period of 40 seconds to generate spatially alternating stimulus pulses of 20 seconds. Simulations with increasing amounts of mechanical feedback were performed for a total of 600 seconds each. The period of the observed pulsatile contraction was measured using a simple Fourier transform as described above.

Modeling the closure dynamics of a contractile ring

To model a closing ring, we implement our reaction-diffusion model on a series of viscoelastic edges initially arranged in a ring of radius R, connected by vertices, with positions x_i. Edge $i$connects vertices $i$and $i+1$and has a tangent vector defined by $t_i = \frac{(x_{i+1}-x_i)}{|x_{i+1}-x_i|}$, with outward normal n_i perpendicular to this. The edge has length $l_i = |x_{i+1} - x_i|$.

Each edge has RhoA concentration r_i and actomyosin concentration m_i which evolve as

$$\dot{r}_i = R_r(r_i, m_i) + \frac{D_r}{l_i}\left(\frac{r_{i+1} - r_i}{\frac{1}{2}(l_{i+1}+l_i)} + \frac{r_{i-1} - r_i}{\frac{1}{2}(l_{i-1}+l_i)}\right) - r_i\frac{\dot{l}_i}{l_i} \quad \text{(Equation 6)}$$

and

$$\dot{m}_i = R_m(r_i, m_i) + \frac{D_m}{l_i}\left(\frac{m_{i+1} - m_i}{\frac{1}{2}(l_{i+1}+l_i)} + \frac{m_{i-1} - m_i}{\frac{1}{2}(l_{i-1}+l_i)}\right) - m_i\frac{\dot{l}_i}{l_i}. \quad \text{(Equation 7)}$$

In each equation, the first term represents the production and degradation rates of RhoA and actomyosin. The second term represents diffusion across neighboring edges, which slows as the center-to-center distance between edges, e.g. $\frac{1}{2}(l_{i+1} + l_i)$, increases. The final term represents the dilution effect due to an expanding or contracting edge. Note that there is no advection term on each edge because the edges themselves move in space.

For the mechanical component, each edge has an active tension $\sigma_i^a = \frac{\sigma_0 m_i}{m_i + m_0}$ which applies contractile forces to both of the edge's vertices, and which increases with actomyosin up to a maximum value of σ_0. Each edge also acts as a spring, with rest length l_i^0 and Young's modulus Eproducing an elastic stress $\sigma_i^e = E\frac{(l_i - l_i^0)}{l_i^0}$. The springs are also viscoelastic, with the rest length remodeling over time $\dot{l}_i^0 = (l_i - l_i^0)/\tau$ at a rate τ^{-1}. Rest length remodeling is a consequence of strain relaxation in the system which arises from actomyosin turnover, such that a local strained element is replaced by an unstrained element over a timescale τ. The resulting force on vertex $i$is then

$$f_i = l_i^0\left(\sigma_i^e + \sigma_i^a\right)t_i - l_{i-1}^0\left(\sigma_{i-1}^e + \sigma_{i-1}^a\right)t_{i-1} \quad \text{(Equation 8)}$$

which is the sum of forces from the two edges connected to the vertex.

Finally, we update the vertex positions through force balance, in which friction balances the active and elastic forces from the contractile ring. We apply an anisotropic friction, such that friction perpendicular to the ring γ_n is higher than friction tangential to the ring γ_t as this gives our simulation more similar results to the experiments. This additional friction could be due to resistance from the cell, for example, moving the ring tangentially doesn't deform the surface of the dividing embryo, while radially contracting the ring does, and so likely has an energy penalty associated with it. Our equation of the motion for each vertex is then

$$\{\dot{x}_i\} = \frac{(f_i \cdot n_i^v)n_i^v}{\gamma_n} + \frac{f_i - (f_i \cdot n_i^v)n_i^v}{\gamma_t} \quad \text{(Equation 9)}$$

where $n_i^v = \frac{(n_i + n_{i-1})}{|n_i + n_{i-1}|}$ is the vertex normal, and we are projecting the force into normal and tangential components.

Within one simulation, we initially fix the radial position of the vertices while allowing for tangential motion and allow the system to evolve for 300s which allows the uniform pulses observed at the start of simulations (Figure 6A) to develop into waves of RhoA. After this period radial motion is allowed again.

The key difference between this and the original model is the implementation of boundary condition (periodic vs closing boundary). If we disallow radial (normal to the ring) motion in the active gel model, then the two models are equivalent up to some reduction in force because some force is inwards into the ring. As the size of the ring gets larger the two models converge.

Please cite this article in press as: Werner et al., Mechanical and biochemical feedback combine to generate complex contractile oscillations in cytokinesis, Current Biology (2024), https://doi.org/10.1016/j.cub.2024.06.037

Figures

Figures were generated using Adobe Illustrator, Python, Microsoft Excel and MATLAB. Beeswarm plots (Figures 3E, 4C, 4D, 5B, 5E, 6D, S4B, S5A–S5C, S6B, and S6C) were generated in Matlab adapting code from Jonas.[114] Weighted histograms (Figures 2C, 3D, 3E, 4E, 5C, S2A, S2B, and S6A) were generated from Matlab scripts from the Matlab central File exchange.[111]

QUANTIFICATION AND STATISTICAL ANALYSIS

Statistical significance was determined using a two-tailed Student's t test or one way ANOVA followed by a Dunnet test for multiple comparison with the same control using corresponding Matlab functions. A p value of less than 0.05 was considered significant. Respective P-values are shown in all figures. All error bars represent standard deviations. Sample size (n) are indicated in the text or the figure legend.